CONTENTS

NASA Contractor Report 3141

Thermal-Structural Design Study of an Airframe-Integrated Scramjet

Summary Report

O. A. Buchmann

CONTRACT NAS1-13984
OCTOBER 1979

NASA

NASA Contractor Report 3141

Thermal-Structural Design Study of an Airframe-Integrated Scramjet

Summary Report

O. A. Buchmann
AiResearch Manufacturing Company of California
Torrance, California

Prepared for
Langley Research Center
under Contract NAS1-13984

National Aeronautics
and Space Administration

**Scientific and Technical
Information Branch**

1973

BLANK PAGE

CONTENTS

INTRODUCTION

The Langley Research Center of NASA has been involved in a research program for the development of airframe-integrated Scramjet concepts. These concepts use the entire undersurface of the aircraft to process the engine airflow. The forebody of the aircraft serves as an extension of the engine inlet and the afterbody serves as an extension of the engine nozzle.

The NASA Hypersonic Research Engine (HRE) program (ref. 1) was a major contributor to the development of Scramjet technology. This program culminated in (1) successful development of the first flightweight, hydrogen-cooled engine structure, including verification tests in the NASA-Langley 8-Foot High-Temperature Structures Tunnel; and (2) confirmation of dual-mode (subsonic/supersonic combustion) aerothermodynamic performance at Mach 5 to 7 in the NASA-Lewis facility at Plum Brook. Baseline data for the current study were also taken from the NASA-sponsored hydrogen-cooled panel studies (refs. 2 and 3).

The current study is an extension of the preliminary thermal-structural design of an airframe-integrated Scramjet conducted by NASA (ref. 4). The objective is to define an engine concept that has a sound basis in materials and manufacturing technology. Emphasis is placed on the engine thermal-structural design, although consideration is given to the fuel subsystem and the aircraft interface. The thermal-structural design evolved in the ref. 4 study and the HRE technology form the basis for this effort. The aerodynamic lines were defined by NASA and remained unchanged during the study. This report summarizes the results of the current study. Details are given in refs. 5 and 6.

Engine design is based on a research-size aircraft to provide a focal point; however, technological development is aimed at eventual commercial applications. The importance of hypersonic technology, its potential applications, and the case for a hypersonic research vehicle are described by Hearth and Preyss (ref. 7). Convectively cooled engine and airframe structures for hypersonic flight are reviewed in ref. 8.

The principal contributors to the study were Messrs. J. J. Killackey (program engineer); E. A. Katinszky, G. D. Mueller, and S. Tepper (structural analysis); A. A. Vuigner and C. C. Wright (thermal and flow analyses); and M. Cooke (mechanical design). Values for the physical quantities are given in both SI and U.S. Customary units. Calculations were made in U.S. Customary units.

Identification of commercial products in this report is to adequately describe the materials and does not constitute official endorsement, expressed or implied, of such products or manufacturers by the National Aeronautics and Space Administration.

SYMBOLS

M_∞	Free-stream Mach number, dimensionless
q_∞	Free-stream dynamic pressure, Pa (psf)
σ_y	Yield stress, Pa (psi)
ϕ_c	Cooling equivalence ratio (fuel used for regenerative engine cooling as fraction of fuel burned), dimensionless

ϕ_f	Fuel equivalence ratio burned, dimensionless
ΔP	Pressure drop, Pa (psi)
ΔT	Temperature difference, K (°R)
T	Temperature, K (°R)
P	Pressure, Pa (psi)
T_{wo}	Temperature at outer (aerodynamic) surface of cooling jacket wall, K (°R)
T_{wi}	Temperature at inner surface of cooling jacket wall, K (°R)
ΔT_w	Temperature difference across cooling jacket wall, $T_{wo}-T_{wi}$, K (°R)

ENGINE DESCRIPTION

A typical installation of the airframe-integrated Scramjet engine on a high-speed airplane is shown in fig. 1. The rectangular modular engine is attached directly to the vehicle undersurface. The aircraft forebody serves as the air inlet compression ramp and the afterbody serves as an extension of the engine nozzle; the entire undersurface is integrated into the engine design. The modular engines provide maximum capture of the airflow between the body and bow shock with minimum external drag.

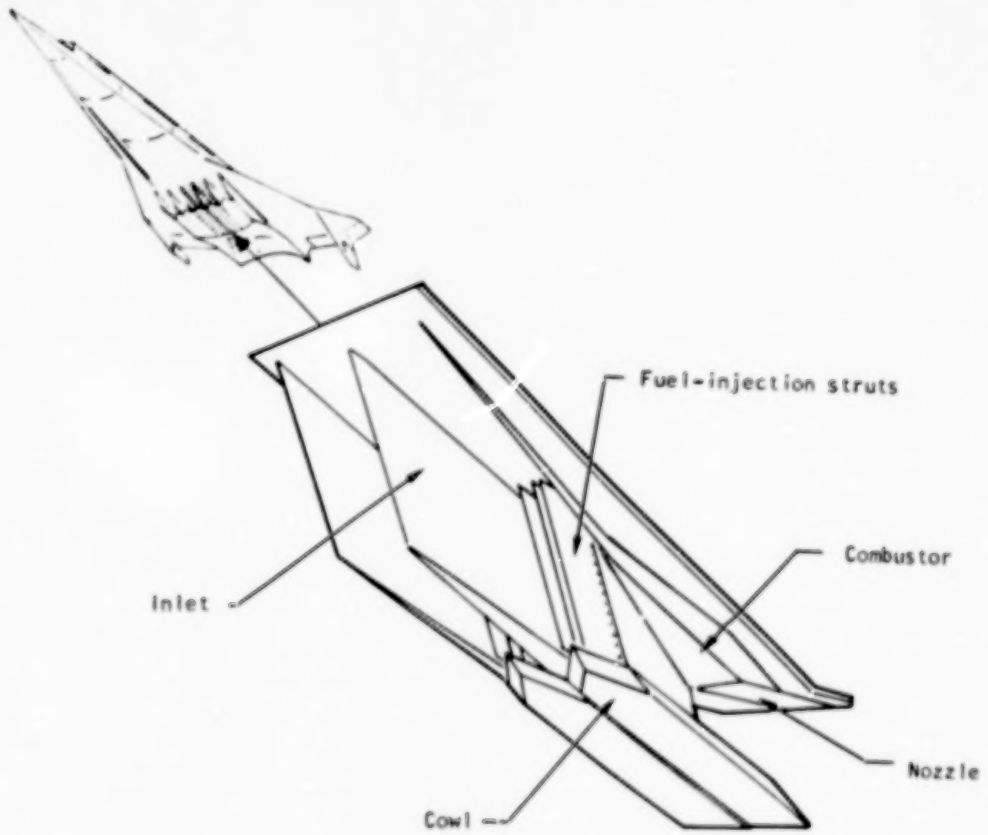

Figure 1. -Scramjet engine configuration and installation.

Two inner Scramjet modules are shown in fig. 1; the sidewall of one module is removed to show the internal engine surfaces. A module for this study was 45.7 cm (18.0 in.) high by 36.6 cm (14.4 in.) wide with an overall length of 314.3 cm (123.7 in.). To provide accessibility and replaceability of parts, each Scramjet module is comprised of four structural panels: topwall, cowl, sidewalls, and three fuel injection struts. The sidewalls of adjacent modules are split, with common leading and trailing edge. This facilitates assembly and accommodates lateral thermal expansion of the modules. The two side struts are identical, have asymmetric cross-sections, and have 3/2 of the chord of the center strut, which has a symmetric cross-section.

The module structural design concept is shown in fig. 2. All engine internal and external surfaces exposed to aerodynamic flow are cooled regeneratively by circulating hydrogen fuel (prior to injection) through a cooling jacket. Coolant is introduced in the inlet and nozzle regions (low heat load) and flows toward the engine throat (highest heat load), where it is collected in manifolds and directed to the fuel plenum. From there, the fuel is routed to manifolds in each strut and injected into the airstream.

Materials proposed in the design are: honeycomb panels (topwall, sidewalls, and cowl), Hastelloy X and Inconel 718; strut primary structure, Inconel 718; stiffening beams, Inconel 718; manifolds and the leading and trailing edge support structure, Hastelloy X; cooling jacket, Nickel-200 and Hastelloy X; and the mounts and mounting frame, Inconel 718.

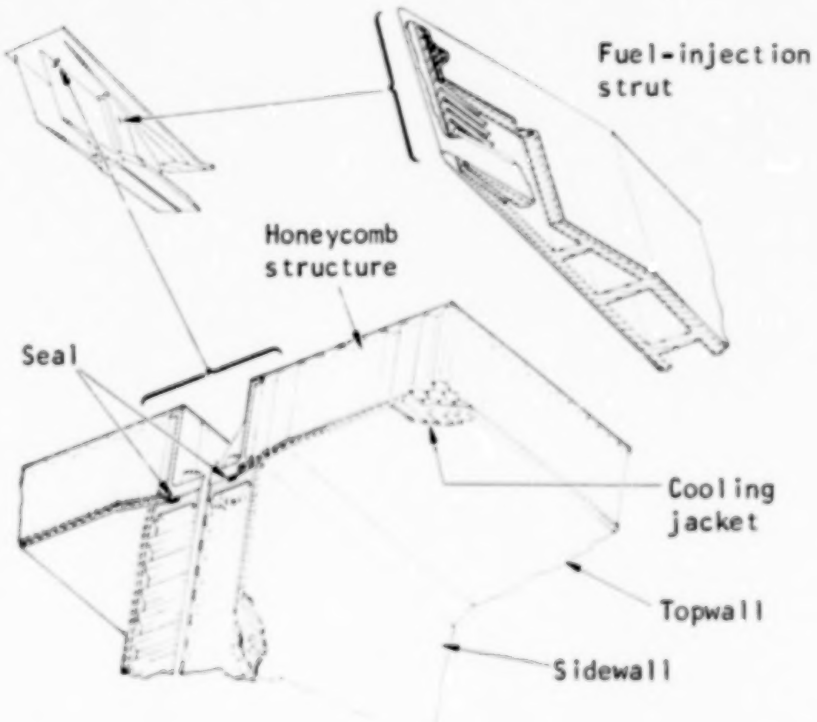

Figure 2. -Salient features of cooled Scramjet structure.

DESIGN CONDITIONS

Normal engine operation is from Mach 4 to 10 with cruise at a dynamic pressure of 23.9 kPa (500 psf) and ascent at a dynamic pressure of 71.8 kPa (1500 psf). The engine also has the capability of undergoing a 2-g powered maneuver within this envelope. The altitude-Mach number envelope for design conditions A through I is shown in fig. 3. It is assumed that the engine can reach steady-state operation at any point within the envelope. Transient conditions such as startup or shutdown can dictate structural design, and are therefore considered in the study.

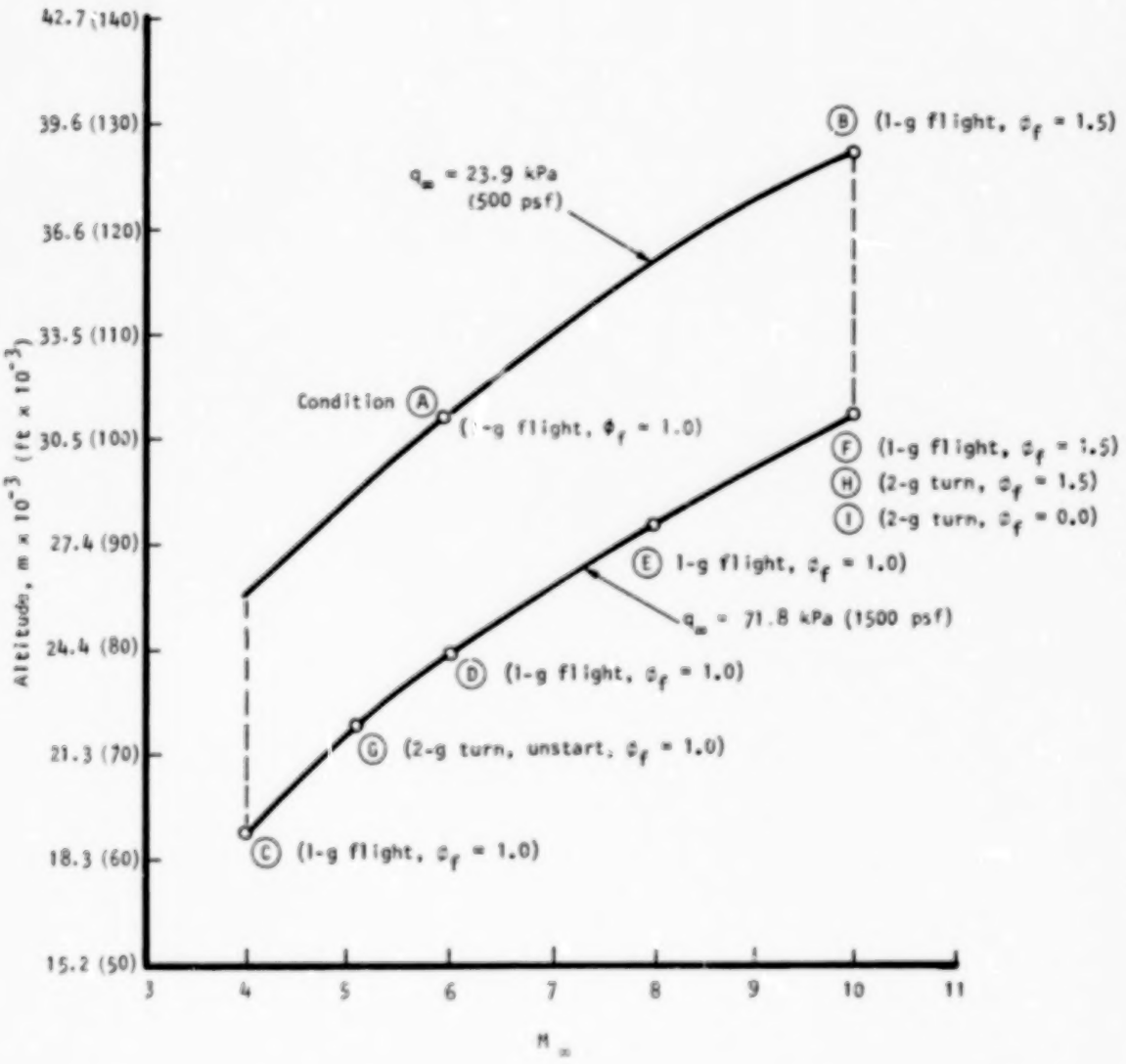

Figure 3. -Altitude-Mach number envelope.

Structural Design Criteria

The basic design objective for the engine is to minimize engine mass and cooling requirements and maintain structural integrity during all flight conditions, including any engine unstarts and any periods of high heat flux to the engine with or without combustion. Design life goals are 100 hours of hot operation with 1000 operational cycles.

In addition, the engine must withstand 10 engine unstarts during the 100-hour lifetime at the maximum aero-pressure loading condition. Thermal and mechanical distortions that occur during normal service are to be limited, to change flow areas by no more than 5 percent or angles by no more than 0.4 deg.

Fuel/Coolant Conditions

The fuel/coolant is parahydrogen stored cryogenically as a liquid at 20 K (37°R) and 138 kPa (20 psia). Hydrogen temperature at the engine inlet is taken as 56 K (100°R) to allow for pump work and aerodynamic heating effects. For maximum utilization of the hydrogen heat sink capability, the design objective is to heat the hydrogen coolant to 890 K (1600°R) (primary structure temperature limit) within any cooling circuit.

The minimum fuel-injection pressure is specified as 4.83 MPa (700 psia) to assure the proper fuel flow rate and penetration into the airstream. The pressure drop across any cooling circuit is assumed to be 1.72 MPa (250 psi), with an additional 0.34 MPa (50 psi) allowed for the control valves and distribution system. The resulting coolant inlet manifold pressure is 6.9 MPa (1000 psia), which is compatible with the pressure containment capability of candidate structures and turbopump delivery pressures. It does not necessarily represent an upper limit for either.

DESIGN LOADING

Aerodynamic Heating

Aerodynamic heating of the internal engine surfaces (sidewall, topwall, cowl), strut sides, and external surfaces was determined for the Condition H maximum thermal load case (fig. 3). The adiabatic wall reference enthalpy method was used to calculate aerodynamic heating rates. Results are presented in fig. 4 for the sidewall only, which is typical of the other components. The integrated heat load for an inboard module is 6.85 MW (6500 Btu/s), and is 7.62 MW (7320 Btu/s) for an outboard module.

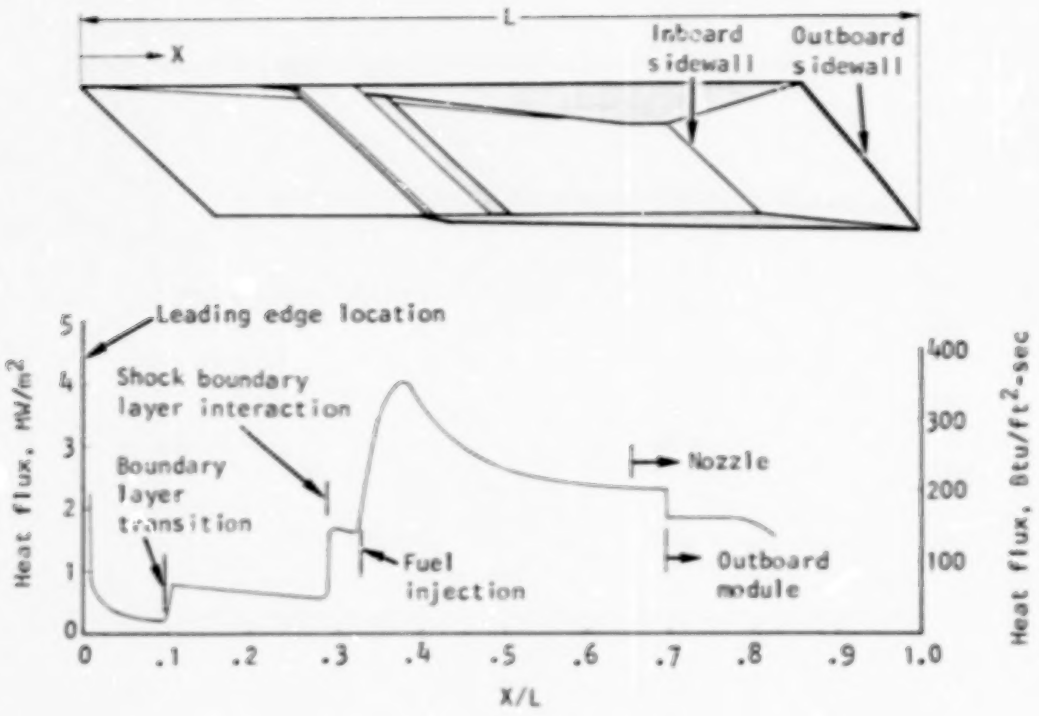

Figure 4. -Aerodynamic heating rates on engine sidewall at the top.

Leading Edge Heat Flux

Leading edge heat fluxes were calculated using the stagnation point method of Fay-Riddell (ref. 9). The normal component of total pressure was used in the calculation of leading edge velocity gradient to account for leading edge sweep angle. The wall temperature at the stagnation line was assumed to be 833 K (1500°R). Radii of 0.8 and 1.3 mm (0.030 and 0.050 in.) were evaluated. The 1.3 mm (0.050 in.) radius was selected; the heat fluxes are listed in Table 3, which is presented in a subsequent section of this report.

Corner Flow Heating

The aerodynamic heating rate in the corners was determined from ref. 10. This indicated that the corner heating was of the same magnitude as on the flat surfaces. It was therefore not a factor in defining cooling jacket configuration and operation.

Pressure Loads

Maximum pressure loads occur in the event of an engine unstart. For design, the unstart is postulated to occur due to thermal choke at Mach 5.2. Typical loads for the sidewall are shown in fig. 5. This loading has the greatest impact on strut design. The integrated strut loads are shown in fig. 6 for the possible combinations. These loads assume that the unstarted pressure acts on the base area of the trailing edge. Because the isobars are vertical on the unstarted side and swept on the started side, a torsional load is produced. Experimental data for the unstart condition are presented in ref. 11.

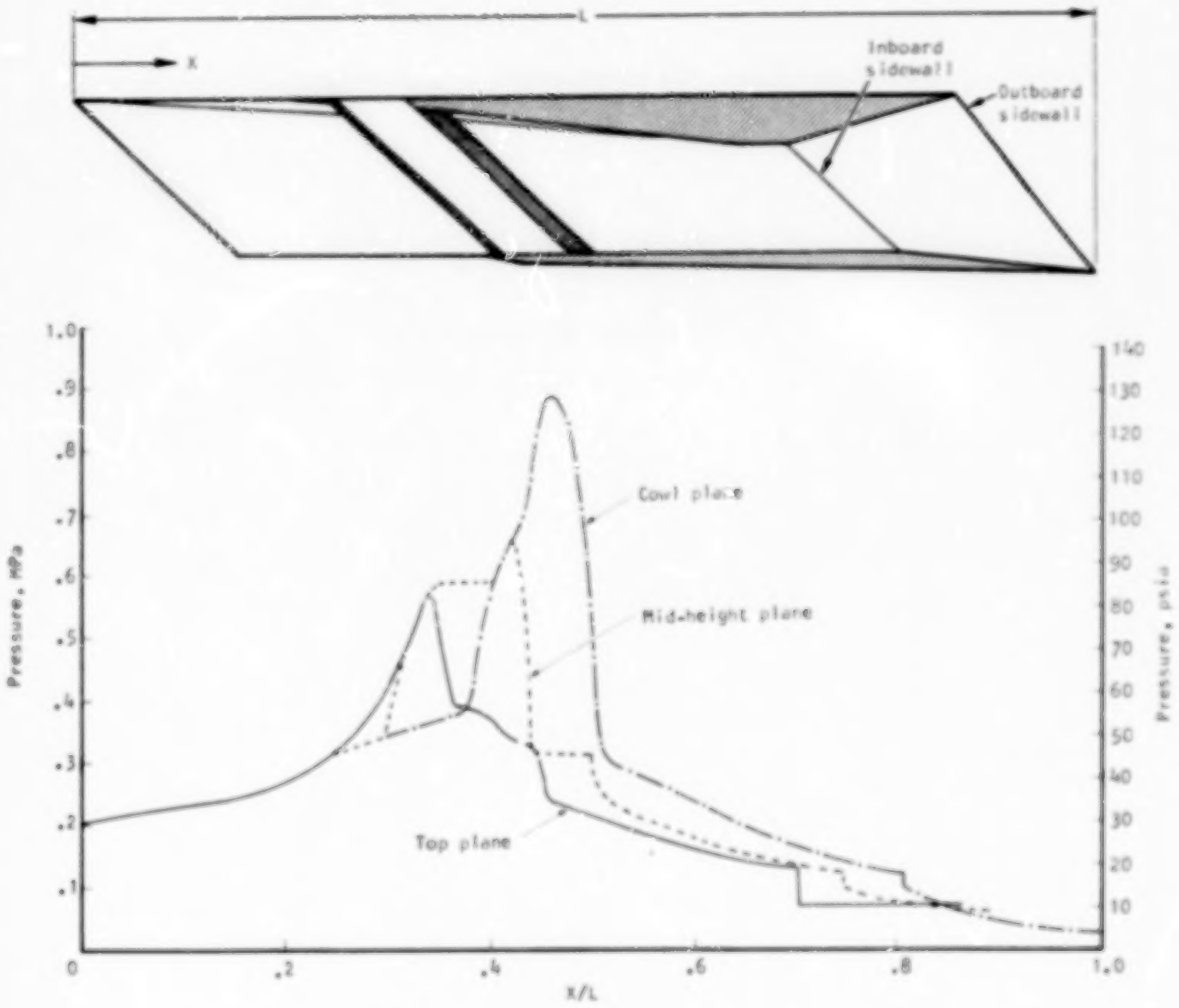

Figure 5. -Engine unstart pressure distributions on the sidewall at three heights

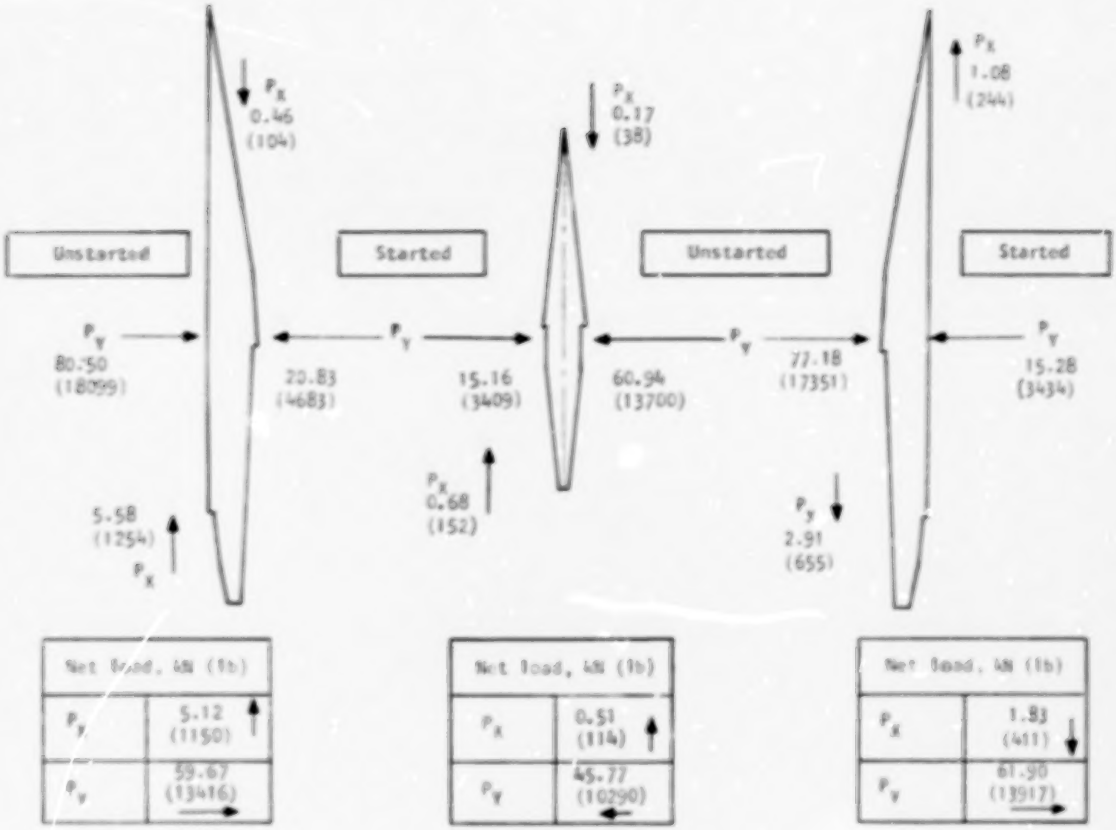

Figure 6. -Strut loads, transient unstart conditions. (Loads are given in kN and parenthetically in lb; arrow indicates direction)

DESIGN AND PERFORMANCE

Material Selection

The study was based on the premise that existing materials and known manufacturing methods will be used. Hastelloy X was selected as the reference material because of an extensive data base and successful application in the Hypersonic Research Engine (HRE) program (ref. 12).

Cooling jacket.--None of the available nickel- or cobalt-base wrought superalloys have a clear-cut superiority, although published properties indicate an advantage for Inconel 617. The data base for Hastelloy X, especially on low-cycle-fatigue (LCF) life, is more extensive than for other alloys; therefore, Hastelloy X was selected where adequate. Because of exceptionally high ductility, Nickel-200 or Nickel-201 are attractive alternates. However, because of low creep strength, the maximum operating temperature must be limited to

1060 K (1910°R) or less. Directly applicable low-cycle fatigue data and high-temperature creep data are lacking. Such data are being obtained as part of NASA Contract NAS1-14180 with the NASA Langley Research Center. Preliminary data are presented in ref. 13.

Primary structure.--The maximum operating temperature for the primary structure is 890 K (1600°R). At this level, inconel 718 is generally optimum because of superior yield strength compared with Hastelloy X or Inconel 617. Fabrication is more difficult with Inconel 718 than with Hastelloy X because of the tendency for welded assemblies to distort during the heat treatment cycle. Consequently, Hastelloy X was selected as a baseline except where the higher strength of Inconel 718 is required.

Coolant Flow Routing

Design conditions.--Coolant inlet and outlet temperatures are 56 and 890 K (100° and 1600°R), respectively. Coolant inlet pressure is 6.9 MPa (1000 psia) and the pressure drop in the actual cooling jacket of any one circuit is limited to 1.4 MPa (200 psi). An added 0.68 MPa (100 psi) total was assigned to manifolding, distribution system, and valving.

Component flow arrangement.--Several routing schemes were investigated. Most of the possible routes produced an excessive pressure drop, excessive temperature gradient, or a sudden step change in skin temperature of greater than 220 K (400°R). The selected coolant flow routing through an engine module is shown in fig. 7. This scheme requires a minimum number of manifolds and the flow is easy to meter because of an adequate pressure drop in each panel. To alleviate temperature mismatch, the four panel outlet manifolds were made coplanar with the swept sidewall manifolds.

The maneuver condition (H) was used as the basis for temperature matching. This is a short-term condition relative to a cruise condition, which is the more applicable condition for temperature matching. Condition H was used, nevertheless, because detailed thermal analysis was performed at this condition and because the results serve to demonstrate the concept.

With the scheme shown in fig. 7, coolant for the entire aft end of the engine is fed through the trailing edges of the cowl and top surface. Redistribution shunt manifolds are located on the top surface and internal cowl surface in line with the trailing edge of the internal sidewall. At this point a portion of the coolant flow is split from the aft top surface and aft internal cowl cooling circuits, and is directed to the side distribution manifold. Flow is directed from this manifold to the aft portion of the sidewall circuits.

A tradeoff analysis using pressure drop and cooling jacket in-depth temperature difference as parameters resulted in an optimum outlet manifold position at $X/L = 0.61$ (at the cowl plane). The in-depth temperature difference proved to be relatively insensitive to small variations in outlet manifold position. The manifold position was therefore selected to minimize the interface

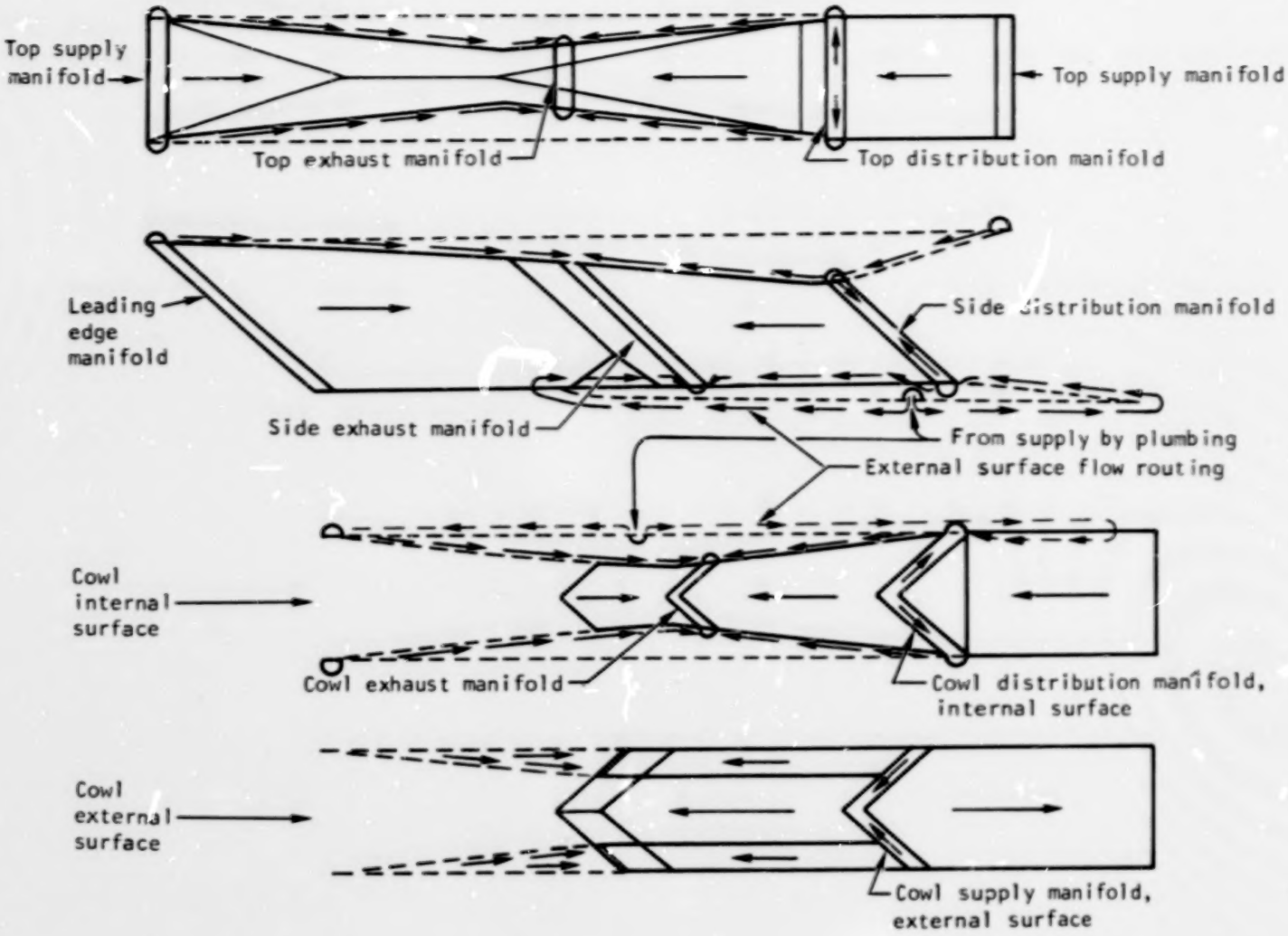

Figure 7. -Engine module coolant routing scheme.

temperature difference between panels, as shown in fig. 8. This represents acceptable primary structure temperature profiles (honeycomb hot face sheet). The maximum interpanel temperature difference at any sweepline position is 120 K (216°R). Coolant flow conditions in each circuit of an inner module for Condition H are defined in fig. 9.

Strut flow routing.--Two strut flow routing schemes were examined: (1) coolant flow parallel to the plane of the cowl; and (2) coolant flow along the 48-deg sweep line. The second scheme did not offer any significant advantages and the resulting flow paths created significant temperature discontinuities. Consequently, the flow routing scheme with the hydrogen coolant flow parallel to the plane of the cowl, as shown in fig. 10, was selected. Coolant flow conditions for the struts are noted in fig. 9.

Flight Envelope Cooling Requirements

To determine engine heat loads at conditions throughout the operating envelope (see fig. 3), the engine was divided into four regions: inlet, combustor, nozzle, and external surfaces. Heat loads at other conditions were determined based on Condition H loads and the particular heat transfer mechanism in each of these regions. The inlet has mostly laminar flow with constant total enthalpy (inlet air); the combustor has turbulent flow with increasing total

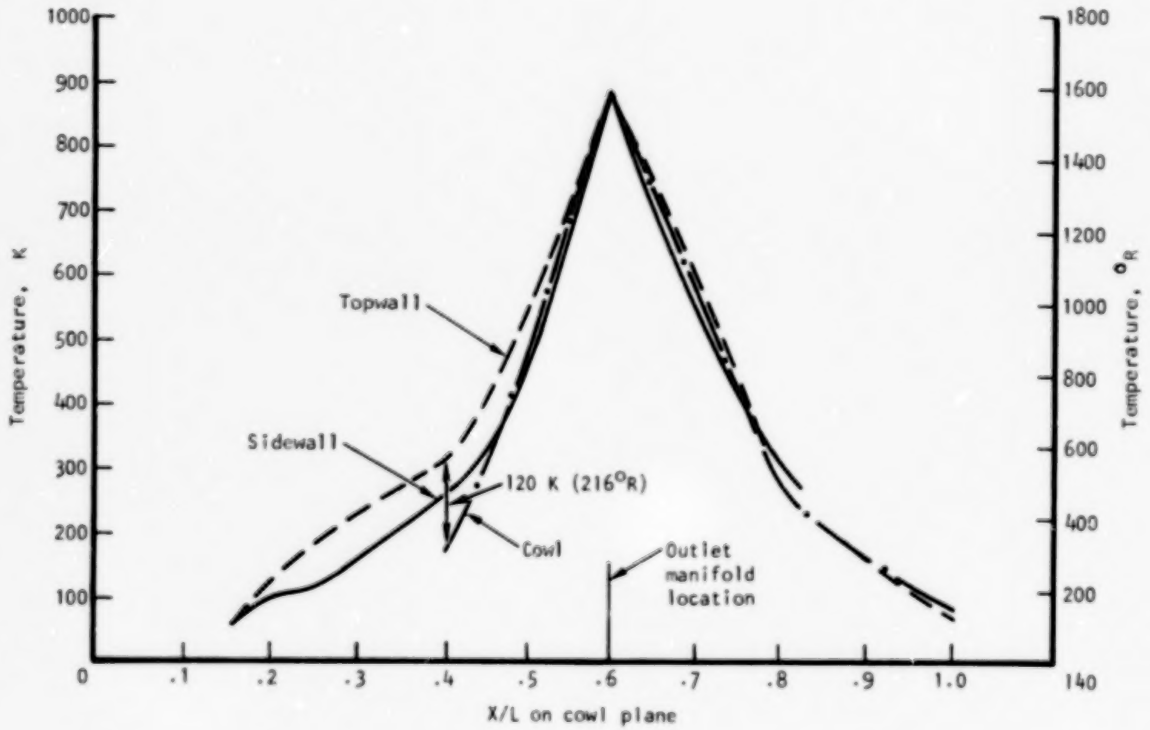

Figure 8. -Primary structure temperature profiles with coplanar outlet manifolds and shunt flow routing.

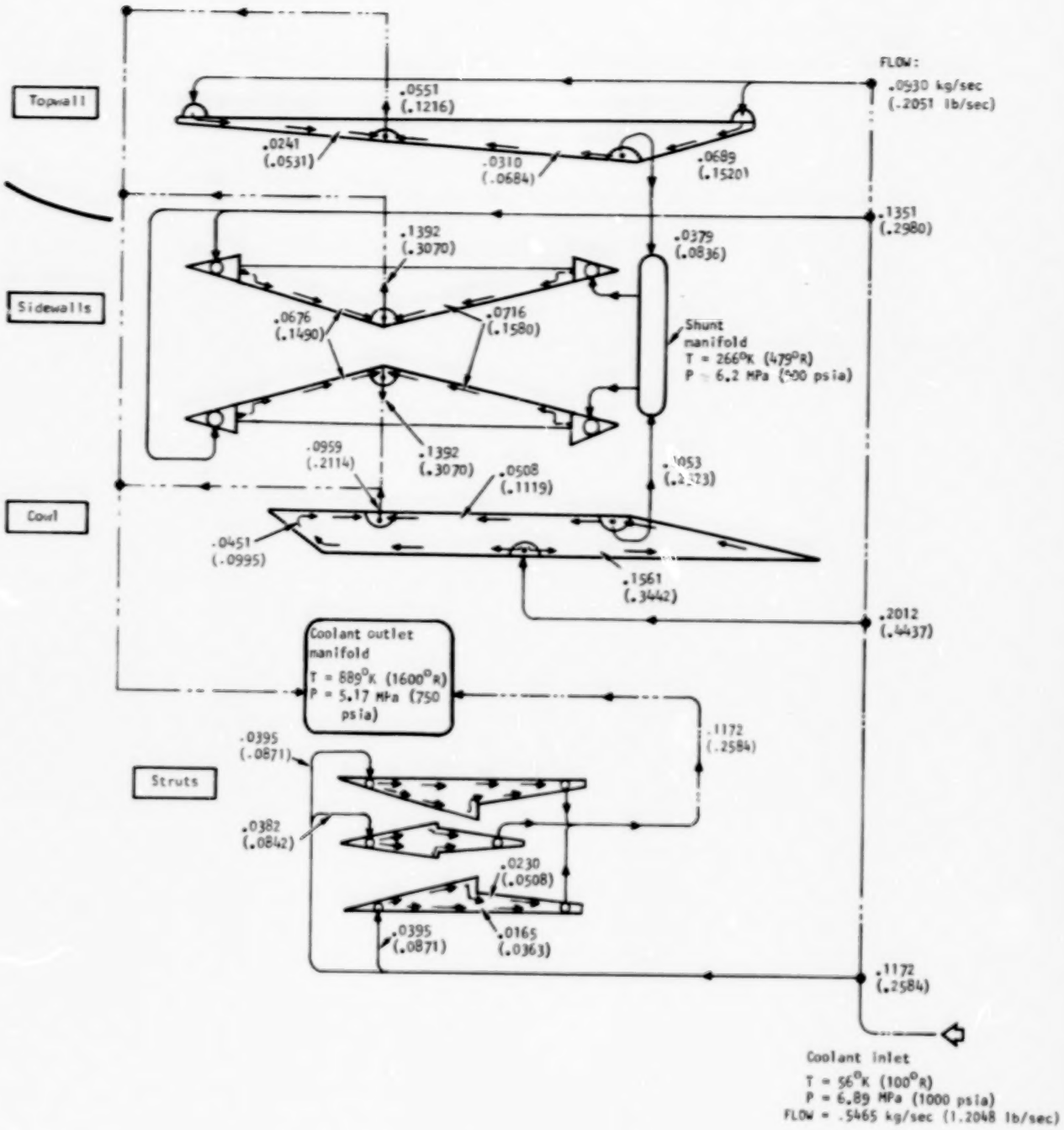

Figure 9. -Coolant flow conditions for inner module.

Figure 10. -Strut coolant flow routing parallel to hot gas flow.

enthalpy (inlet air to combustion products); the nozzle has turbulent flow with constant total enthalpy (combustion products); and the external surfaces have mostly turbulent flow with constant total enthalpy (inlet air). The calculations included the average effect of mass velocity, wall temperature, and hot gas fluid properties in each region.

Results are presented in Table 1 for an inboard module, an outboard module, and a six-module cluster (four inboard and two outboard modules). Minimum hydrogen coolant flow rates were established assuming that the coolant is heated from 56 K (100°R) to 890 K (1600°R) except for Condition A'. For this condition, all fuel was routed through the coolant circuits. The inlet temperature was increased until this total flow was heated to the 890 K (1600°R) maximum fluid outlet temperature and the cooling equivalence ratio, ϕ_c, was equal to 1.0. For this cruise condition, the coolant supply temperature may be increased to 420 K (756°R), which indicates that 44 percent of the coolant heat capacity is available for airframe cooling. These coolant rates are considered minimum because of inherent inefficiencies in the cooling system.

The coolant equivalence ratios, ϕ_c, in Table 1 are based on fuel flows for stoichiometric combustion at all operating conditions. The coolant requirements were determined from conditions listed in fig. 3, with ϕ_f = 0, 1.0, and 1.5. The fuel equivalence ratio, ϕ_f, of 1.5 is not used since it applies only to the selected design point for a research airplane. It is required to provide adequate thrust in this application and is not appropriate to a commercial airplane. The values given in Table 1 for ϕ_c at ϕ_f = 1.0 assume that the heat load and coolant flow are unchanged in going from ϕ_f = 1.5 to ϕ_f = 1.0. The maximum and minimum ϕ_c, which occur at Conditions B and C, respectively, reflect their extreme positions on the altitude-Mach number envelope (fig. 3).

The fraction of the stoichiometric fuel flow required to cool the Scramjet engine at two dynamic pressures is shown in fig. 11 as a function of Mach number. The fuel provides an adequate heat sink for cooling the engine at Mach numbers up to approximately 9 at a dynamic pressure of 24 kPa (500 psf) and to even higher Mach numbers at a dynamic pressure of 72 kPa (1500 psf). The cooling requirements are less severe at the higher dynamic pressure because the heat load increases as the 0.8 power of the dynamic pressure, while the fuel requirement increases linearly. At lower Mach numbers there is surplus hydrogen fuel heat sink for airframe and/or additional engine cooling.

TABLE 1.-ALTITUDE-MACH NUMBER ENVELOPE COOLANT REQUIREMENTS.

Flight condition (Fig. 3)	Inboard module heat load, MW (Btu/s)	Outboard module heat load, MW (Btu/s)	Six module heat load, MW (Btu/s)	Inboard module coolant flow, kg/s (lbm/s)	Outboard module coolant flow, kg/s (lbm/s)	Six module coolant flow, kg/s (lbm/s)	Inboard/ outboard module fuel flow, kg/s (lbm/s)	Six module fuel flow, kg/s (lbm/s)	Inboard module, cooling equiv. ratio, ϕ_c (ϕ_f = 1.0)	Outboard module, cooling equiv. ratio, ϕ_c (ϕ_f = 1.0)	Six module ϕ_c at ϕ_f = 1
A	1.48 (1407)	1.73 (1640)	9.39 (8908)	.118 (.261)	.138 (.304)	.748 (1.650)	.245 (.540)	1.470 (3.240)	.483	.563	.509
A'	1.48 (1407)	1.73 (1640)	9.39 (8908)	.245 (.540) T_{in} = 486 K (876°R)	.249 (.540) T_{in} = 420 K (756°R)	1.47 (3.240) T_{in} = 464 K (836°R)	.245 (.540)	1.470 (3.240)	1.000	1.000	1.000
B	3.58 (3399)	4.04 (3835)	22.42 (21266)	.285 (.629)	.322 (.710)	1.79 (3.936)	.365 (.804)	2.188 (4.824)	1.173	1.324	1.239
C	1.13 (1075)	1.44 (1366)	7.41 (7032)	.090 (.199)	.115 (.253)	.591 (1.302)	.584 (1.287)	3.503 (7.722)	.155	.197	.169
D	2.87 (2719)	3.31 (3135)	18.08 (17146)	.229 (.504)	.264 (.581)	1.44 (3.175)	.607 (1.339)	3.644 (8.034)	.376	.434	.395
E	4.06 (3855)	4.60 (4361)	25.45 (24142)	.324 (.714)	.367 (.808)	2.03 (4.471)	.581 (1.280)	3.484 (7.680)	.558	.631	.582
F	5.75 (5454)	6.41 (6076)	35.81 (33968)	.458 (1.010)	.510 (1.125)	.285 (6.290)	.828 (1.826)	4.970 (10.956)	.829	.924	.861
G	2.70 (2562)	3.16 (2993)	17.12 (16234)	.215 (.474)	.251 (.554)	1.36 (3.006)	.667 (1.471)	4.003 (8.826)	.332	.377	.341
H	6.85 (6500)	7.72 (7319)	42.85 (40638)	.546 (1.205)	.615 (1.355)	3.41 (7.526)	1.007 (2.220)	6.042 (13.320)	.813	.915	.848
I	3.25 (3078)	3.88 (3680)	20.74 (19672)	.259 (.570)	.309 (.681)	1.65 (3.643)	0.0	0.0	-	-	.410

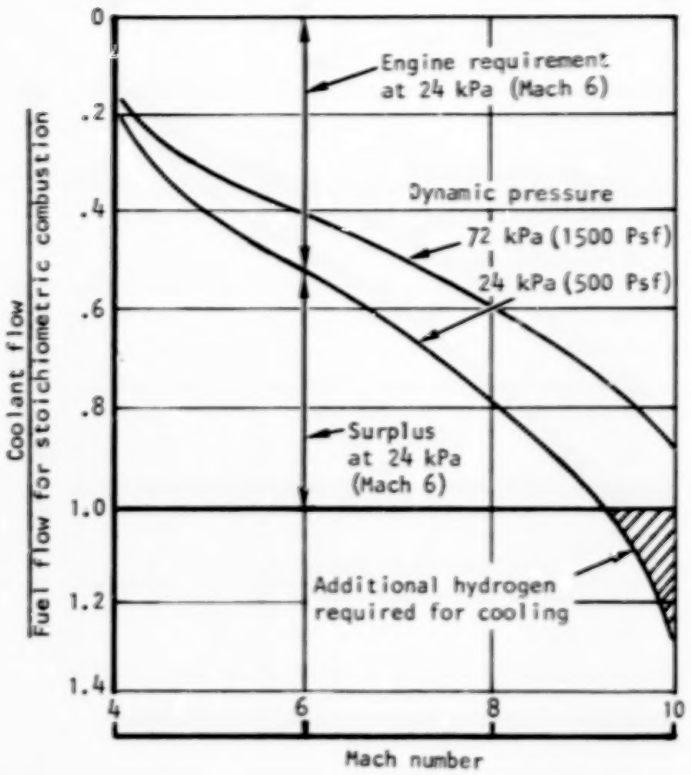

Figure 11. -Engine cooling requirements.

Thermal Protection System (TPS)

Coolant passage design.--Three types of coolant passage configurations were considered: (1) rectangular offset plate-fin, (2) rectangular plain machined channel, and (3) circular pin-fin. A sketch of each configuration and the dimensional ranges considered are shown in fig. 12. Pin-fins were selected for the struts and machined channels for all other components. The pin-fins provide the increased heat transfer performance required in the struts, as compared with straight channels; the associated increase in unit pressure drop is acceptable because of the short flow lengths.

The cooling performance of each configuration was determined at average hydrogen flow conditions for each flow route. Coolant pressure drop was estimated for the entire flow route; the temperature difference across the coolant passage was determined only at the peak heat flux condition or location.

Passive as well as active schemes were investigated for external surface cooling. With insulation, the net heat load to the structure is low but still must be absorbed by some means. The primary drawback to passive cooling is that the hot substrate must be attached to the cooler engine structure, leading to heat conduction to the primary structure, potentially serious soak back, and thermal stress problems. Since the coolant requirement is only approximately 5 percent more than ideally obtainable with use of insulation and the above problems are eliminated, active cooling was selected for the external surfaces.

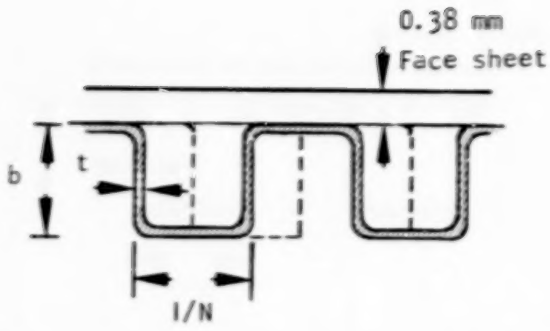

N = fins per cm of flow width

Fins considered:

(1) N = 11, b = 1.3 mm, t = 0.15 mm

(2) N = 14, b = 0.64 mm, t = 0.05 mm

(a) Rectangular offset plate-fin

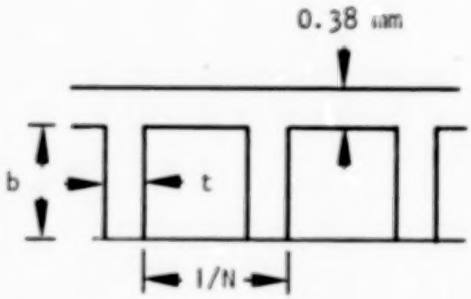

Dimensions considered:

l/N = 2.0 mm

t = 0.5 mm

b = 0.64 and 1.27 mm

(b) Machined channel

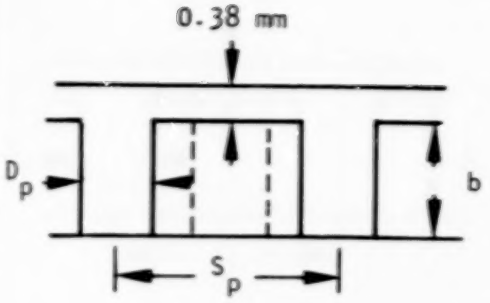

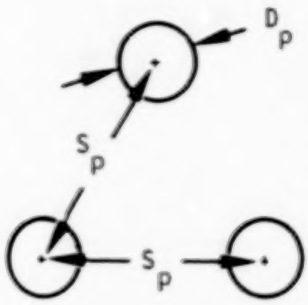

Dimensions considered:

S_p = 2.0 mm

D_p = 0.76 and 1.02 mm

b = 0.64, 1.27, 1.91 mm

(c) Pin-fin

Figure 12. -Coolant passage configurations.

Fatigue Life.--The primary structure is cool relative to the aerodynamically heated face sheet of the cooled passage and limits the thermal expansion of the heated face sheet, which is less stiff. This results in repetitive elastic-plastic loading cycles that cause accumulated damage and eventual failure by low-cycle fatigue (LCF). The LCF life of the candidate configuration was determined by finite element analysis.

Final selections and estimated performance for the cooling jackets are presented in Table 2. The following criteria were used: (1) cooling jacket pressure drop including any shunt circuits must be less than 1.38 MPa (200 psi); (2) Hastelloy X is used except where coolant passage in-depth temperature difference exceeds 222 K (400°R); (3) Nickel-200 is used in high heat flux areas where Hastelloy X is not suitable; and (4) maximum cooling jacket face sheet temperature must be less than 1144 K (2060°R) for Hastelloy X and 1060 K (1910°R) for Nickel-200.

The coolant passage geometry is not critical for external engine surfaces. A machined channel is recommended because of its greater structural stiffness, low temperature gradients, and compatibility with the other coolant passage geometries.

Leading Edges

Coolant routing.--Two basic coolant routing schemes for the leading edges were considered: impingement, direct and indirect; and parallel-flow. The configuration for direct impingement cooling is shown by the solid lines in fig. 13.

TABLE 2. -COOLING JACKET PERFORMANCE.

Flow circuit	Configuration	Material	Cooling jacket in-depth temperature difference, K (°R)	Maximum skin temperature, K (°R)	Total ΔP, MPa (psi)	Cycle life
Cowl, forward	Channel, 0.64 mm deep	Nickel	169 (305)	423 (761)	0.76 (110)	5000 +
Cowl, aft*	Channel, 0.64 mm deep	Hastelloy X	202 (363)	1102 (1983)	1.07 (155)	1450
Side, forward	Channel, 0.64 mm deep	Nickel	135 (243)	685 (1233)	0.70 (101)	10,000 +
Side, aft	Channel, 0.64 mm deep	Hastelloy X	178 (320)	1078 (1940)	1.24 (180)	1820
Top, forward	Channel, 0.64 mm deep	Hastelloy X	146 (263)	608 (1094)	0.35 (51)	5000 +
Top, aft	Channel, 0.64 mm deep	Hastelloy X	119 (215)	1019 (1835)	0.65 (94)	5000 +
Strut, center	Pin-fin, 1.0 mm dia by 0.64 mm deep	Nickel	167 (300)	1011 (1820)	0.33 (48)	2500 +
Strut, side	Pin-fin, 1.0 mm dia by 0.64 mm deep	Nickel	138 (249)	1038 (1869)	0.79 (114)	4000 +

*External cowl and nozzle portions of the topwall and internal cowl utilize a 1.27-mm-deep channel surface.

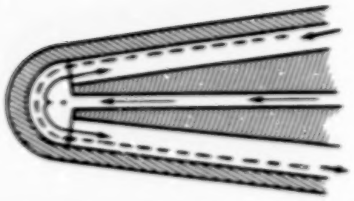

Figure 13. -Coolant routing for direct impingement cooling of leading edges.

With indirect impingement, the flow turns nearly 180 deg (less the wedge angle), as indicated by the dashed lines in fig. 13. This produces a near-impingement cooling effect.

In the parallel-flow concept, the coolant flows in a channel just behind and parallel to the leading edge. This concept was eliminated because the skin temperature difference and pressure drop are higher than for impingement cooling, and the flow routing is not compatible with the longitudinal flow routing of the engine panels.

Heat transfer performance.--Results for impingement cooled schemes are summarized in Table 3. Metal temperatures presented are for the stagnation point with 0.38-mm (0.015-in.)-thick Hastelloy X. Except for the first 2.5 mm (0.1 in.) or length, overall coolant circuit performance is similar for either direct or indirect impingement cooling, and therefore is not a factor.

TABLE 3. -LEADING EDGE THERMAL PERFORMANCE WITH HASTELLOY X.

Leading edge	Heat flux, MW/m² (Btu/s-ft²)	Indirect impingement			Direct impingement					
					Parallel to hot gas flow			Normal to sweep flow		
		T_{wo}, K (°R)	T_{wi}, K (°R)	ΔT_w, K (°R)	T_{wo}, K (°R)	T_{wi}, K (°R)	ΔT_w, K (°R)	T_{wo}, K (°R)	T_{wi}, K (°R)	ΔT_w, K (°R)
Sidewall	10.61 (935)	758 (1365)	464 (835)	294 (530)	587 (1057)	313 (564)	274 (493)	560 (1008)	286 (515)	274 (493)
Cowl	14.36 (1266)	582 (1048)	211 (380)	371 (668)	681 (1226)	310 (558)	371 (668)	- -	- -	- -
Cowl apex	45.84 (4042)	1364 (2456)	440 (792)	924 (1664)	- -	- -	- -	1494 (2690)	639 (1150)	855 (1540)
Center strut	20.25 (1792)	1261 (2270)	835 (1503)	426 (767)	1125 (2025)	599 (1079)	526 (946)	1052 (1893)	527 (948)	525 (945)
Side strut	15.04 (1331)	1037 (1867)	657 (1165)	390 (702)	901 (1621)	511 (919)	390 (702)	840 (1512)	394 (710)	446 (802)

Note: Temperatures are for conditions at the stagnation line. Heat fluxes are shown for T_{wo} = 833 K (1500°R)

Direct impingement cooling produces the highest heat transfer coefficients, resulting in the lowest leading edge temperatures. For the cowl and cowl apex, indirect impingement is used for compatibility with the overall coolant flow routing and flow route temperature profiles. The sidewall, cowl, and side strut leading edge temperatures appear to be acceptable, although temperature differences are high. Performance at the cowl apex is unsatisfactory with Hastelloy X. Nickel-200 was therefore considered for use here and to increase the cycle life of other leading edges.

Cycle life analysis.--The estimated leading edge cycle life is given in Table 4. The strain range partitioning technique (refs. 14, 15, and 16) with a safety factor of 4 was used. Typical material properties and a strain concentration factor of 2.0 were specified. For Hastelloy X, the temperature data presented in Table 3 were used directly. For Nickel-200, the data in Table 3 were ratioed by the thermal conductivities to estimate the operating temperatures. The results lead to the following conclusions:

(a) Cycle life requirements can be met by using Nickel-200 material for all leading edges including the cowl apex.

(b) Direct impingement cooling should be used for the sidewalls and struts because it produces superior cycle life.

TABLE 4. -LEADING EDGE CYCLE LIFE.

Location	Impingement cooling mode	Cycle life with candidate materials	
		Hastelloy X	Nickel-100
Sidewall	Direct	2800	10,000
	Indirect	500	-
Cowl	Indirect	1000	16,000
Cowl apex	Indirect	40	1400
Side strut	Direct	400	2600
	Indirect	300	-
Center strut	Direct	-	-
	Indirect	150	1700

Although Nickel-200 is the recommended material, its creep strength is low. The selection of Nickel-200 is based on the use of general LCF correlations (refs. 14, 15, and 16). To confirm this selection, both detailed mathematical modeling and experimental evaluation of the long-term behavior of the leading edge structure with combined creep and fatigue loading are required. Consideration must also be given to the degradation of material properties in the braze-affected zone. Relevant basic experimental data on Nickel-200 is being obtained under NASA Contract NAS1-14180 (ref. 13).

Fuel-Injection Struts

Hydrogen manifolding and flow distribution.--The fuel and coolant can be routed through the struts either by separate lines within the strut structure or by using the strut structure itself to contain the hydrogen.

The approach using separate lines to contain the fuel and coolant was considered as a means of simplifying the overall plumbing arrangement and minimizing thermal stresses. This approach proved impractical. The limited flow areas available with tubes would have required manifolding from both ends of the struts--a formidable design problem given the restrictive envelope in the cowl.

The integral manifold approach evaluated in ref. 4 was found to be effective. The key feature in the design is a thermal buffer (a layer of stagnant hydrogen) that reduces the internal convection heating from the hot hydrogen in the manifolds. The resulting thermal stresses are reasonable.

As part of the present study, flow distribution and pressure drop in the fuel injector manifolds, the coolant manifolds, and the cooling jackets in the center and side struts were analyzed in detail. In addition, the fuel injector nozzles were sized, and heat transfer coefficients in all flow passages were computed for use in future analyses. Fig. 14 shows the selected manifold

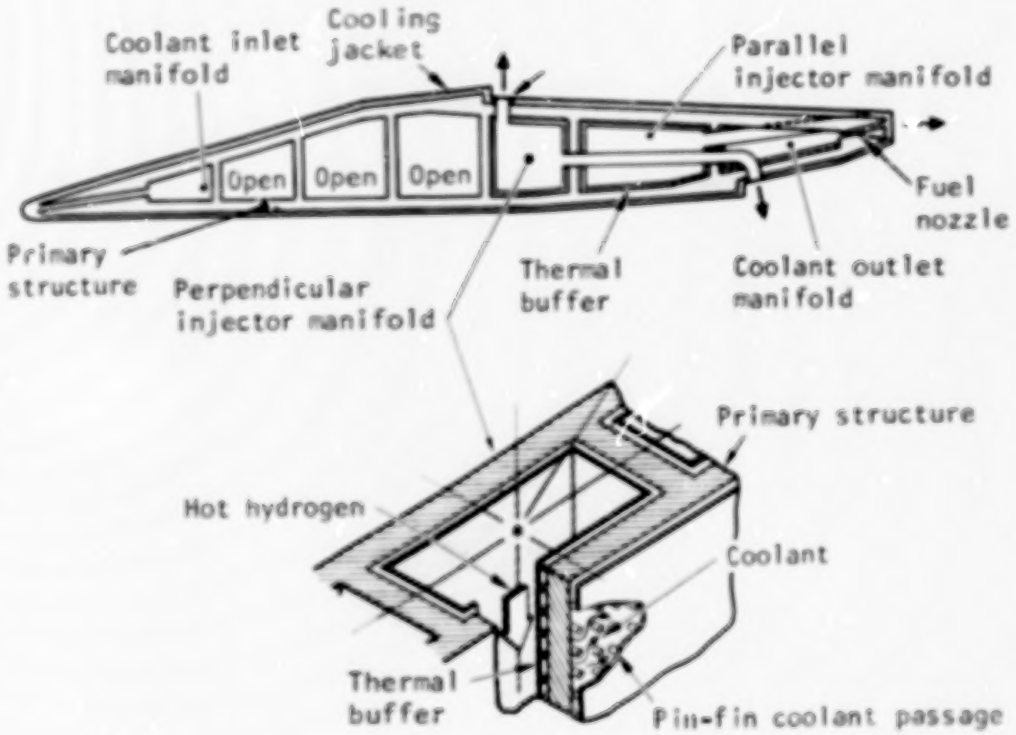

Figure 14. -Side strut configurations and cooled wall structure.

and structural configuration for a side strut. Satisfactory flow distribution can be obtained in all of the fuel and coolant manifolds. With constant diameter fuel nozzles, the nozzle flows varied a maximum of ±7 percent from the average flow. The maximum coolant maldistribution was 11 percent and occurred in the cooling jacket of the side strut.

Side strut structural analysis.—Structural analyses conducted by NASA (refs. 4 and 8) indicated an excessive stress level within the side strut when subjected to an unsymmetrical unstart condition. A possible solution is to tie the struts together at midspan, thereby decreasing the bending stresses due to the external side load by a factor of 2. Analysis and design showed that a midspan tie is structurally and aerodynamically feasible; however, the resultant complications in coolant flow routing and strut fabrication are substantial. It is also recognized that the data used in establishing the loading condition are uncertain. Means for reducing the thermal loading were therefore considered as an alternate approach to reduce the combined loading without resorting to a midspan tie.

Figs. 14 and 15 illustrate the selected strut configuration and mounting provisions. Bulkheads, 2.5 mm (0.100 in.) thick, resist bending and separate the coolant and fuel manifolds. To mount the strut in the topwall, a hinge is used; in addition, the strut is installed in a peripheral seal plate that forms part of the topwall and provides restraint of strut deformations.

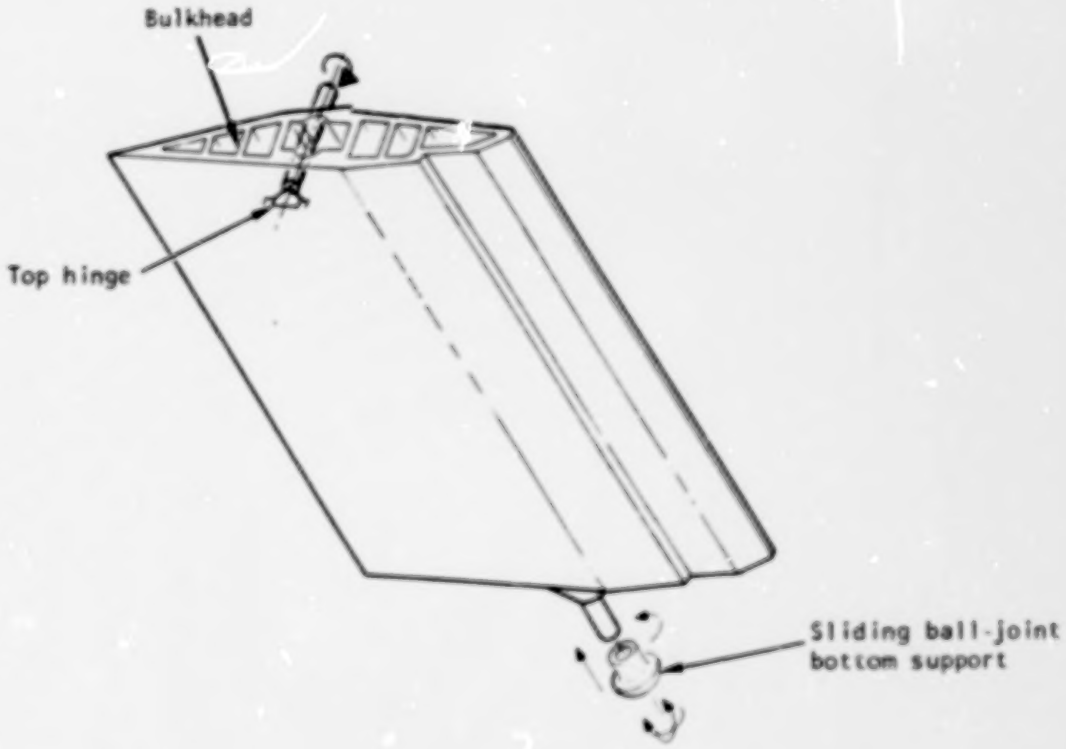

Figure 15. -Strut mounting.

The thermal loading of the struts was reduced by reducing the coolant outlet temperature of the struts to 417 K (750°R) from 889 K (1600°R). This results in increasing the strut coolant flow by a factor of 2. The increased flow at Condition G is then about equal to the maximum coolant flow at Condition H with an 889 K (1600°R) coolant outlet temperature. The overall engine coolant at Condition G is increased by about 20 percent. This relatively large overall increase results from the need to match structural temperature and from the limited flow control available in individual routes for the selected coolant system concept. The required excess coolant is available at Condition G and other potential unstart conditions ($M_\infty \leq 5.2$), as shown in fig. 11.

The NASA SPAR computer model of the strut was used to analyze the stresses associated with the selected configuration and mounting (ref. 17). The overall conclusion from this analysis is that the midspan tie can be eliminated. Restraint of strut deformation by the topwall mounting and operation with increased coolant flow (i.e., reduced temperature) permit this.

A further detailed structural analysis was performed of a side strut and the wall regions surrounding it under maximum symmetrical unstart loading. This analysis was specifically aimed at assessing the performance of the seal at the interface of the side strut and the topwall. Analysis with various strut-mount clearances indicates that an initial, as-installed mount clearance of 0.51 mm (0.020 in.) is adequate to accommodate thermal expansion differences. The resulting seal requirements are also consistent with the design concept shown on the drawings in ref. 6.

Primary Structure

Three-dimensional finite element models.--The reference-design primary structure used a combination of beam and honeycomb to contain the high-pressure airflow. The concept included seven beams located parallel to the engine sweep line. Two other structural concepts were considered in this study. The first is similar to the reference design except that the beams are oriented vertically (normal to the airflow). The second is an all-honeycomb design in which most of the beams are eliminated in favor of a thicker honeycomb structure.

The following elements are typical for all structures:

Honeycomb front face sheet	1.5 mm (0.060 in.) thick
Honeycomb back face sheet	1.3 mm (0.050 in.) thick
Honeycomb cell	6.4 mm (0.25 in.) hexagon, 0.08 mm (0.003 in.) gauge

A constant 9.5-mm (3/8-in.)-thickness honeycomb is used for all panels in the swept and vertical beam models except for the external cowl and sidewall panels, which are 6.4 mm (1/4 in.) thick. Distribution of honeycomb thickness for the all-honeycomb design is defined in fig. 16. For the all-honeycomb design, the model was based on the assumption that the panel-to-panel intersections are rigidly connected and that there is a continuous honeycomb structure around the corner. The actual design used stiffened corner brackets, as shown in fig. 2.

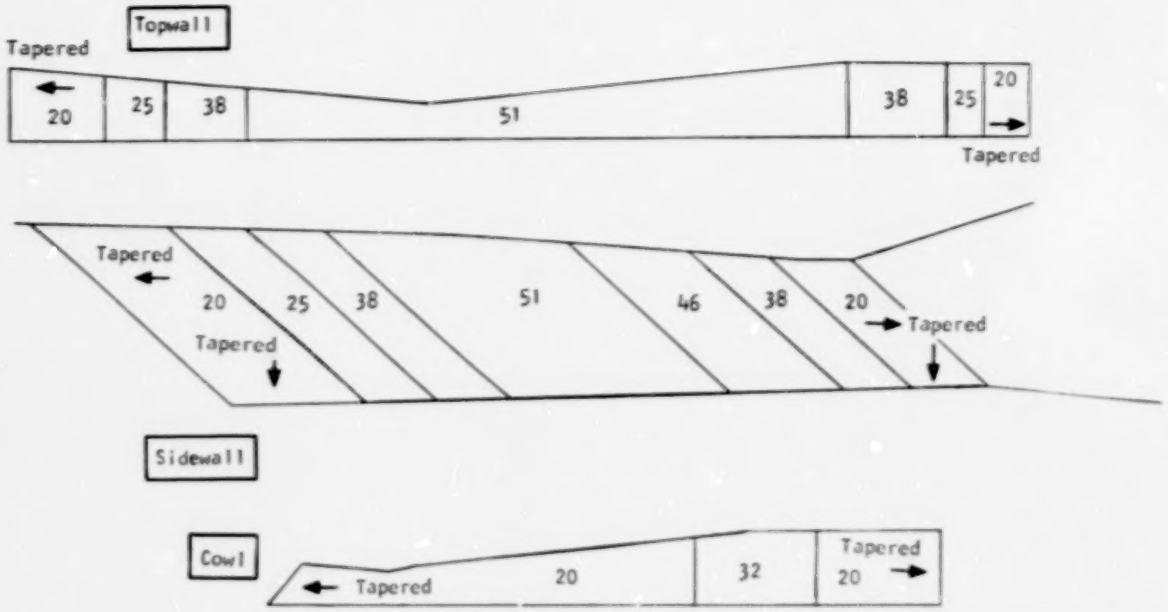

(dimensions in mm)

Figure 16. Honeycomb thickness variation (all-honeycomb model).

Displacement and stress results for the sidewall are shown in fig. 17. The sidewall design is especially critical in terms of displacement of the unsupported leading edge area. The all-honeycomb design is superior to the others in this regard.

Mass comparison.--Estimated mass was determined for each structural design using layout drawings as a basis and the dimensions of the individual parts as used in the finite element analysis. Results for a six-module cluster are 1320 kg (2909 lb) for the swept beam design, 1306 kg (2879 lb) for the vertical beam design, and 1270 kg (2800 lb) for the all-honeycomb design. The honeycomb design has the least mass, but the differences are not considered especially significant.

Design selection.--The honeycomb configuration was selected as the best design primarily because (1) it exhibits the least deflection in the sidewall and nozzle areas--an order of magnitude lower than the beam models; (2) it is the least complex structure--minimum beams and clips; and (3) it has a lower mass than the beam models. A reduced number of beams is desirable because the beams act as a restraint to thermal growth and thereby increase thermal stresses.

Structure	Maximum thermal load		Maximum pressure load	
	Displacement, mm (in.)	Comparative stress MPa, (ksi)	Displacement, mm (in.)	Comparative stress MPa, (ksi)
Swept beam	5.1 (.20)	496 (72)	55 (2.29)	469 (68)
Vertical beam	3.3 (.13)	414 (60)	27 (1.08)	593 (86)
Honeycomb (shown)	0.5 (.02)	248 (36)	5.8 (0.23)	400 (58)

Figure 17. -Displacement and stress results for the sidewall.

Transient analysis.--Temperature gradients in the structure during transient conditions, e.g., at engine ignition, may control structural design. The structure was therefore analyzed to assess the magnitude of the transient temperature gradients and their effect on the selected design concepts.

The mission profile selected for the analysis is shown in fig. 18. The acceleration and deceleration profiles were selected because they are typical of a research airplane, would represent the first application of the engine, and give the worst-case thermal transient load. These profiles were combined with a 1-hr cruise to provide the most severe overall mission. An estimate of the coolant temperature is shown in fig. 19. Combustion occurs at 120 s. At this same instant, the coolant flow is doubled because the heat load with combustion is about twice the value without combustion. The inverse of these operations occurs during deceleration. The transient study focused on the coolant outlet manifold, which experiences the largest temperature gradients and the highest temperatures. The engine thermal response in this region will be one-dimensional except at the corners that join the topwall to the sidewall and the sidewall to the cowl. Since the corner of a module was expected to be critical, all cross-sections analyzed were taken in this area. The topwall-sidewall corner section that was modeled on a thermal analyzer program and the temperature nodal locations are illustrated in fig. 20.

Fig. 21 shows the temperature history at zone 1 (see fig. 20). The front is the hot face sheet of the cooling jacket, and the back is the unheated back face sheet of the honeycomb, which is as much as 5 cm (2 in.) from the hot face sheet. Hastelloy X and nickel were investigated for the honeycomb core. For the face sheet, whether the core is nickel or Hastelloy, the response is extremely fast. At the startup (fig. 20a), the front sheet very quickly reaches 890 K (1600°R), resulting in a front-to-back ΔT of 670 K (1200°R) for a Hastelloy core. At shutdown (fig. 20b), the temperature relationships of the front of the cooling jacket and the back of the honeycomb are reversed. The front-to-back ΔT developed is somewhat less than at startup--on the order of 550 K (1000°R) with a Hastelloy core.

Temperatures from the transient thermal analysis at 140 s into startup, at steady state, and at 80 s into shutdown were input into a finite element structural analysis of the manifold area. The structural analysis, using the (ANSYS) computer program, predicted strain levels that would produce fatigue life below the design objective of 1000 cycles regardless of the material used for the honeycomb core. As noted above, these results are for the extremely severe transient for the rocket-propelled, research vehicle application. It is believed that acceptable life can be obtained for the much less severe commercial application by a combination of material change and changes in the mission trajectory and coolant and fuel scheduling. Studies also indicate that acceptable ΔT's can be obtained, even for the research application, by modifying the cooling jacket design to transport heat to the unheated face sheet; however, this approach adds unwanted complexity to the engine design.

Fig. 22 shows the sidewall structural temperature distribution along the engine axis at 125 s into the assumed mission (fig. 18). (The assumptions were slightly different than those used for the previous analysis, resulting

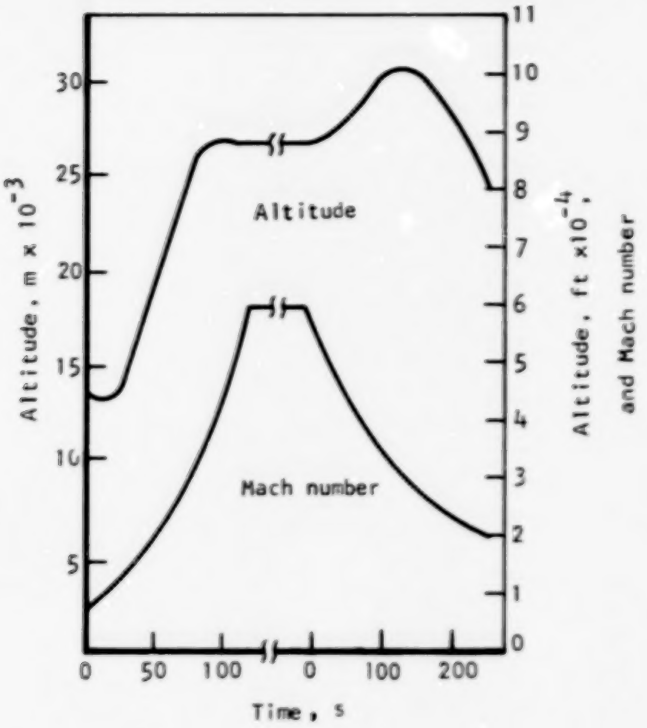

Figure 18. -Mission profile for transient analysis.

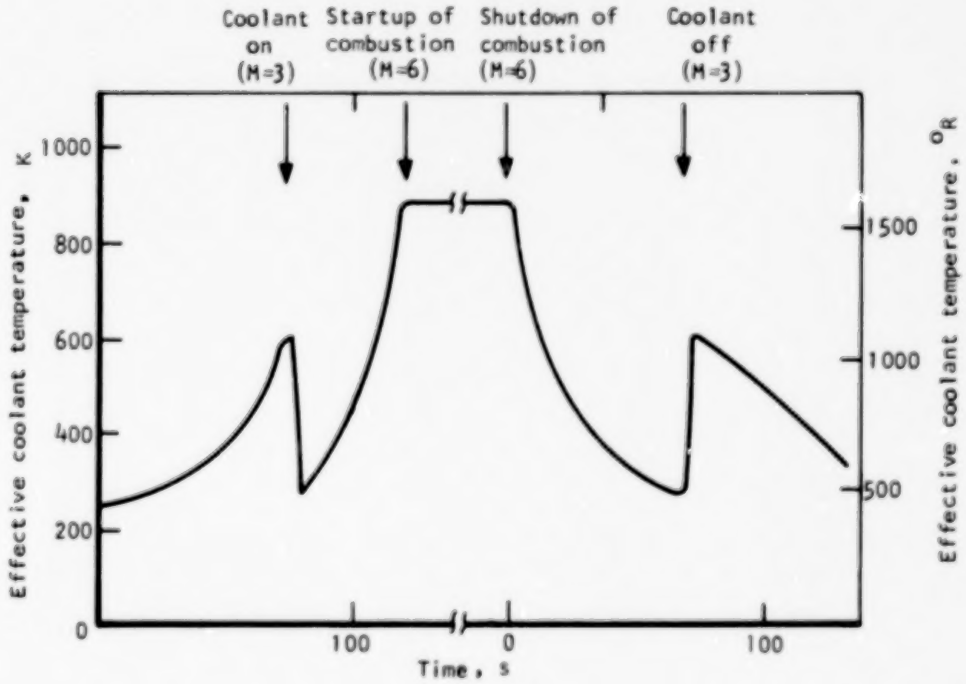

Figure 19. -Estimated coolant outlet temperature history.

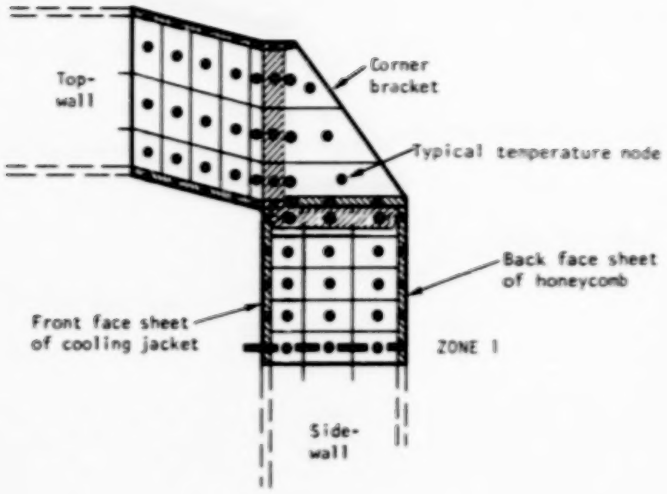

Figure 20. -Schematic and nodal locations for honeycomb transient thermal analysis of topwall-sidewall corner section.

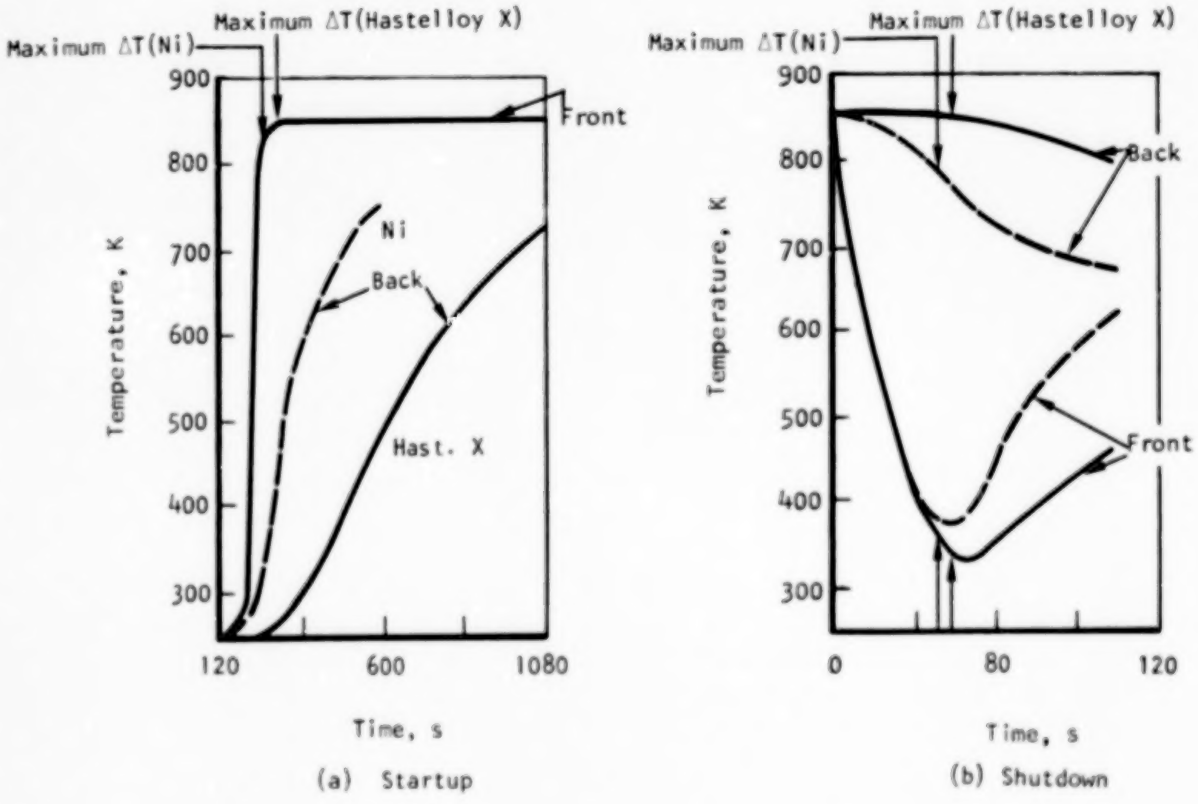

Figure 21. -Honeycomb temperature history at zone 1.

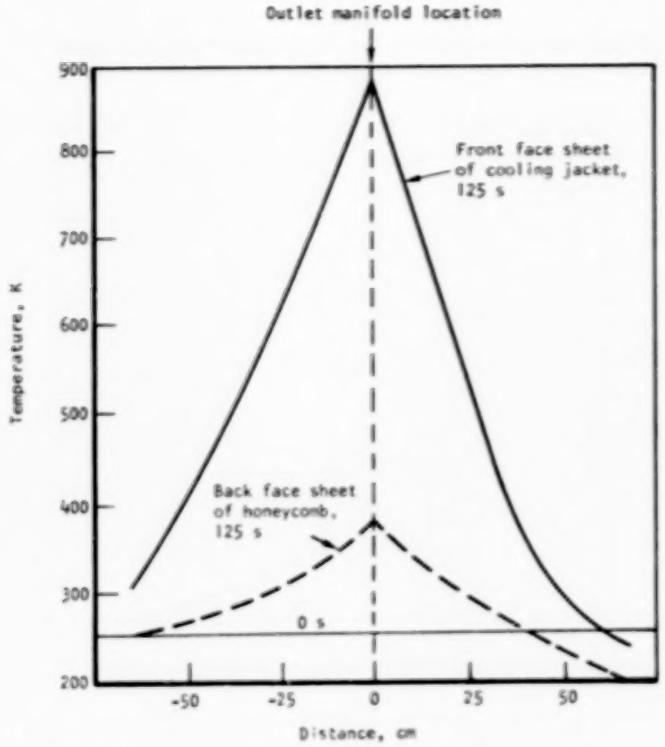

Figure 22. -Typical honeycomb temperatures.

in somewhat different values.) At 125 s into startup, the maximum front-to-back ΔT is 500 K (900°R). It falls off fairly sharply with distance from the outlet manifold. At about 46 cm (18 in.) from the outlet manifold, front-to-back ΔT's are at steady-state values and are acceptable. Design solutions aimed at reducing front-to-back ΔT are only required over an approximately 1 m length. The rest of the engine will be controlled by steady-state front-to-back ΔT's that have been found compatible with the design goals.

ENGINE-AIRCRAFT INTERFACE

A separate mounting frame is used to join the engine modules to the aircraft. The use of a separate frame allows assembly of the individual engine modules and installation on the airplane as a single cluster. This also minimizes the number of engine-aircraft attachment points and permits accommodation of peculiarities in engine module mounting versus aircraft installation requirements. Module loads are transmitted through the topwall honeycomb structure to the mounting frame. The selected concept is shown in fig. 23. In this case, six modules comprise the engine assembly. The frame is rectangular with cross-members at the module split lines. Inconel 718 was selected as the preferred material. It was assumed that the maximum temperature of the mounting frame would not exceed 589 K (1060°R). This temperature is based on calculations made for the HRE environment and assumes the use of flow baffles to limit convective heating by leakage flow in the engine compartment.

As shown in fig. 23a, the engine modules have two mounting points on the frame. Provisions for module thermal growth are shown in fig. 23b. The aft mount is fixed axially, but accommodates accumulative lateral expansion by sliding. The forward mount permits free axial expansion and again accommodates lateral expansion by sliding. An alternative to accommodation of lateral expansion is to absorb it in the split sidewalls.

Fig. 23c shows the concept for accommodating thermal growth differentials between the engine mounting frame and the aircraft structure. The mounting frame is fixed axially at the forward attachment. Lateral growth is accommodated by pivots. The aft attachment accommodates lateral growth by means of pivots and axial growth by sliding connections.

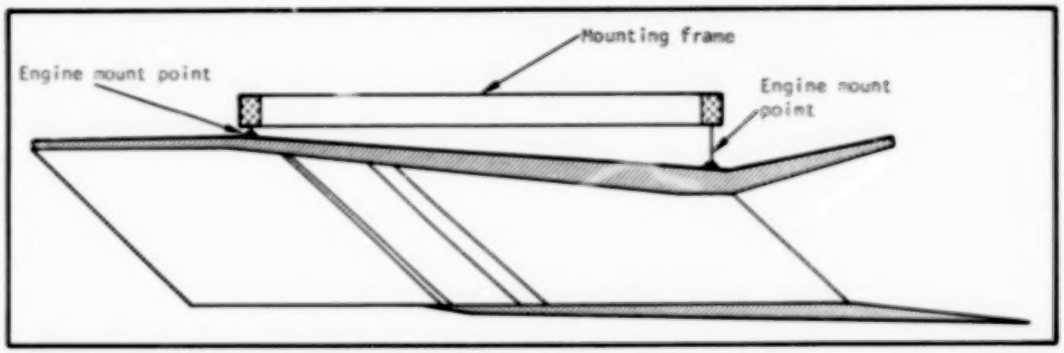

(a) Mounting frame spacing

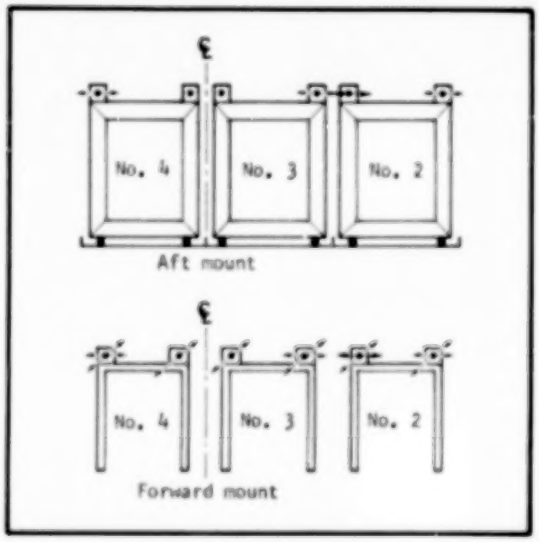

(b) Provisions for module thermal growth

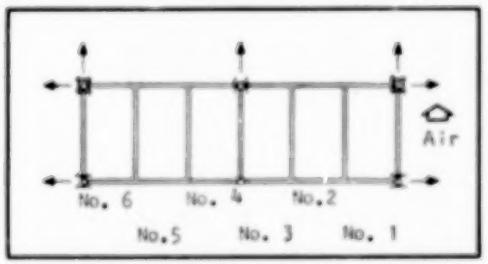

(c) Provisions for mounting-frame thermal growth

Figure 23. -Engine mounting concepts.

Although the engine is modularized, the use of common sidewall leading and trailing edges and the generally limited access prevent separation of a single module assembly from the engine cluster. Repair of an individual panel, except for the external cowl, will also require removal of the engine assembly from the aircraft. Strut removal is through the topwall only. Access to the cowl interior and the space between sidewalls with the engine installed on the aircraft is possible by removing a panel on the external cowl.

HYDROGEN FLOW CONTROL

Coolant Flow Routing

As previously discussed, the proportion of the total heat load absorbed by any individual flow circuit is not constant throughout the flight envelope. To achieve maximum coolant utilization, active controls will be required to maintain the coolant outlet temperature close to the 890 K (1600°R) limit. The number of controls (coolant flow regulating valves) is dependent on how closely the 890 K (1600°R) limit must be met. A number of valves will be required to ensure that the desired interpanel temperature differentials are not exceeded and that the matching is close to that shown in fig. 8.

The least complex approach is to valve all forward-flow routes in parallel and all aft-flow routes in parallel among the six modules. A third valve controls all strut flow routes. This concept divides the engine into three sections: (1) the inlet section, (2) the combustor/nozzle section, and (3) the struts. It is assumed that during normal operation there is no large difference in heating rate between modules and that the heat load split between panels will remain in a reasonably fixed proportion for all flight conditions. Calibrated orificing can then be used to establish the basic flow split between the topwall, sidewalls, and cowl within the forward and aft circuits.

No provision has been made in this concept to cut off coolant or fuel flow to a single module in the event of an unstart or other abnormal condition. Instead, this type of control is provided only for each group of three modules. Since the transient conditions in the engine are severe for even normal operation, operation without combustion in one of the modules may prove feasible for the basic design. Control system response, in turn, may be too slow to prevent the imposition of the large temperature differences associated with combustion shutdown in one module. Additional valving would be of no benefit in such a case. Further detailed study will be required to evaluate the effects of abnormal conditions on both the engine structure and control system configuration. Since such abnormal conditions are strongly mission dependent, they were not evaluated in detail in this study.

Fuel System

A preliminary study was conducted to define the Scramjet fuel system. Estimates of component size and mass were made. To permit selection and sizing of the turbopump system, it was assumed that the equipment would be used in a research airplane with 40 s of cruise at Mach 6.

All hydrogen lines have been sized on the basis of a total fuel flow for six modules of 3.85 kg/s (8.5 lb/s) and a single-module fuel flow of 0.644 kg/s (1.42 lb/s).

A schematic diagram of the fuel system is shown in fig. 24. The modules are grouped in two sets of three. Each set of three modules has a turbopump, coolant regulating valves, and fuel valves. This arrangement permits testing either a three- or six-module cluster on the research airplane, and can also be used to provide redundancy during ground and flight testing.

CONCLUDING REMARKS

The overall objectives of this study were to: (1) develop and evaluate a design concept for the cooled structures assembly for the Langley Scramjet engine; (2) develop concepts for engine subsystems in sufficient detail to show feasibility and estimate mass, volume, and operating requirements; and (3) establish design concepts for the aircraft/engine interface.

The work was organized into tasks aimed at providing the specific thermal-structural and subsystem data needed to meet the study objectives, including: (1) aerodynamic thermal loading definition, (2) conceptual design, (3) optimization and tradeoff, and (4) engine design and performance. Such factors as fabrication, assembly and sealing of components, maintenance and servicing, materials, flutter, buckling, thermal stress, and fatigue were considered in the study.

Overall objectives for the Scramjet engine design can be met. The design life of 100 hr and 1000 cycles is attainable once the temperature differences during transients are controlled. The coolant equivalence ratio for stoichiometric combustion is less than one at Mach numbers up to approximately 9 at a dynamic pressure of 24 kPa (500 psf) and to higher Mach numbers at higher dynamic pressures. The mechanical design is feasible for manufacture using conventional materials. For the cooled structures in a six-module engine, the mass per unit capture area is 1328 kg/m^2 (272 lb/ft^2). The total mass of a six-module engine assembly including the mounting (63.5 kg, 140 lb), the fuel/coolant system (245 kg, 540 lb), and plumbing and instrumentation (136 kg, 300 lb) is 1778 kg (3920 lb). All masses include 5 percent design allowances.

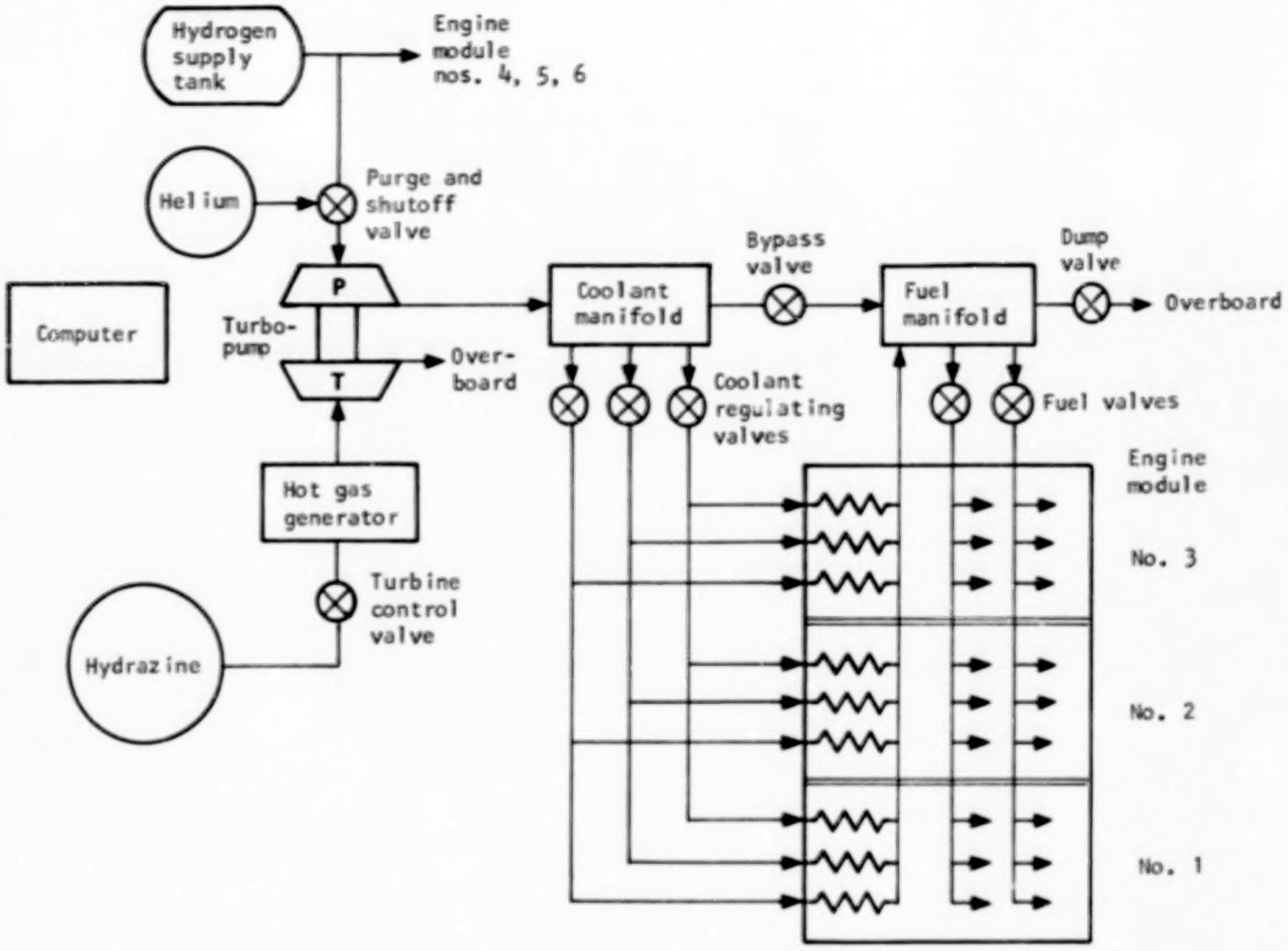

Figure 24. -Schematic of engine fuel system.

An all-honeycomb primary structure has less deflection and complexity than beam and honeycomb combinations of equal mass. The engine panels, i.e., the topwall, sidewall, and cowl, may be rigidly joined at the corners and no dynamic hot gas seals are required. Selected materials are: honeycomb primary structure--Inconel 718; cooling jackets--Hastelloy X or Nickel-200; and leading edges--Nickel-200.

The transient performance of the cooling jacket and structure during engine startup and shutdown may govern the design. For the most severe assumptions concerning mission trajectory and engine operating procedures, based on a research application, in-depth temperature differences can range to 670 K (1200°R). Stresses will be less severe for commercial-type applications where acceleration to cruise is slower. Reduction of temperature differences to acceptable levels is possible by changes in operating procedures and, if required, in design of the cooling jackets.

Design of the engine will benefit from additional data in critical areas. These include: (1) dynamics associated with transient unstart and normal operation because of their effect on the structure and controls requirements; (2) aerodynamic interaction of one module with the next module; (3) better definition of the distribution of heat flux in the combustor, of the shock patterns, and of corner heating; (4) the effect of leading edge blunting to 1.27 mm (0.05 in.) on performance; and (5) the aerodynamic interaction of the aircraft and the engine as it affects thermal-structural design of the engine itself and of the interfaces with an airplane.

REFERENCES

1. Staff of Langley Research Center and AiResearch Manufacturing Company, The Garrett Corporation: Hypersonic Research Engine Project Status, 1971. NASA TM X-2572, 1972.

2. Flieder, W. G., Richard, C. E., Buchmann, O. A., and Walters, F. M.: An Analytical Study of Hydrogen Cooled Panels for Application to Hypersonic Aircraft. NASA CR-1650, April 1971.

3. Richard, C. E., Duncan, J. D., Gellersen, E. W., and Demogenes, C.: Thermal and Structural Tests of a Hydrogen Cooled Panel. NASA-CR-2105, May 1972.

4. Wieting, Allan R., and Guy, Robert W: Thermal-Structural Design/Analysis of an Airframe-Integrated Hydrogen-Cooled Scramjet. J. of Aircraft, Vol. 13, No. 3, March 1976, pp. 192 to 197.

5. Killackey, J. J., Katinszky, E. A., Tepper, S, and Vuigner, A. A.,: Interim Summary Report, Thermal-Structural Design Study of an Airframe-Integrated Scramjet. NASA CR-145368, December 1978.

6. Killackey, J. J., Tepper, S., Mueller, G. D., and Vuigner, A. A.: Final Report, Thermal-Structural Design Study of an Airframe-Integrated Scramjet, NASA CR-159039, 1979.

7. Hearth, Donald P., and Preyss, Col. Albert E., USAF: Hypersonic Technology--Approach to an Expanded Program. Astronautics and Aeronautics, Vol. 14, No. 12, Dec 1976, pp. 20 to 37.

8. Kelly, H. Neale, Wieting, Allan R., Shore, Charles P., and Nowak, Robert J.: Recent Advances in Convectively Cooled Engine and Airframe Structures for Hypersonic Flight. 11th Congress of the International Council of the Aeronautical Sciences, Lisbon, Portugal, Sept. 10 to 16, 1978.

9. Fay, J. A., and Riddell, F. R.: Theory of Stagnation Point Heat Transfer in Dissociated Air. J. of Aeronautical Science, Feb. 1959, p. 17.

10. Stainback, P., and Weinsten, L.: Aerodynamic Heating in the Vicinity of Corners at Hypersonic Speeds. NASA TN D-4130, Nov. 1967.

11. Wieting, Allan R.: Exploratory Study of Transient Unstart Phenomena in a Three-Dimensional Fixed Geometry Scramjet Engine. NASA Technical Note TN D-8156, March 1976.

12. Staff of AiResearch Manufacturing Company, The Garrett Corporation: Hypersonic Research Engine Project, Structures and Cooling Development, Final Technical Data Report. NASA CR-112087, May 1972.

13. Buchmann, O. A.: Advanced Fabrication Techniques for Cooled Engine Structures. Recent Advances in Structures for Hypersonic Flight. NASA CP-2065, 1978, pp. 145-193.

14. Manson, S. S.: The Challenge to Unify Treatment of High Temperature Fatigue--A Partisan Proposal Based on Strainrange Partitioning. Fatigue at Elevated Temperatures, ASTM STP 520, American Society for Testing and Materials, 1973, pp. 744 to 782.

15. Spera, D. A.: Comparison of Experimental and Theoretical Thermal Fatigue Lives for Five Nickel-Base Alloys. Fatigue at Elevated Temperatures, ASTM STP 520, American Society for Testing and Materials, 1972, pp. 648 to 657.

16. Halford, G. R., Hirschberg, H. M., and Manson, S. S.: Temperature Effects on the Strainrange Partitioning Approach for Creep Fatigue Analysis. Fatigue at Elevated Temperatures, ASTM STP 520, American Society for Testing and Materials, 1973, pp. 658 to 669.

17. Wieting, Allan R. and Thornton, Earl A.: Thermostructural Analysis of a Scramjet Fuel-Injection Strut. Recent Advances in Structures for Hypersonic Flight. NASA CP-2065, 1978, pp. 119-144.

1. Report No. NASA CR-3141	2. Government Accession No.	3. Recipient's Catalog No.
4. Title and Subtitle SUMMARY REPORT THERMAL-STRUCTURAL DESIGN STUDY OF AN AIRFRAME-INTEGRATED SCRAMJET		5. Report Date October 1979 6. Performing Organization Code
7. Author(s) O. A. Buchmann		8. Performing Organization Report No. 78-15442-1 10. Work Unit No.
9. Performing Organization Name and Address AiResearch Manufacturing Company of California A Division of The Garrett Corporation 2525 W. 190th Street Torrance, California 90509		11. Contract or Grant No. NAS1-13984
12. Sponsoring Agency Name and Address National Aeronautics and Space Administration Washington, D.C. 20546		13. Type of Report and Period Covered Contractor Report June 1975 to December 1978 14. Sponsoring Agency Code

15. Supplementary Notes

Langley Technical Monitor: Allan R. Wieting
Final Report

16. Abstract

The overall objectives of this study were to: (1) develop and evaluate a design concept for the cooled structures assembly for the Langley Scramjet engine; (2) develop concepts for engine subsystems in sufficient detail to show feasibility and estimate mass, volume, and operating requirements; and (3) establish design concepts for the aircraft/engine interface. Results of the study show that the objectives for the Scramjet engine can be met. A thermal protection system has been defined that makes it possible to attain a life of 100 hours and 1000 cycles, which is the specified goal. With stoichiometric combustion, the fuel provides an adequate heat sink for cooling the engine at Mach numbers up to 9 at the minimum fuel flow condition. The mechanical design is feasible for manufacture using conventional materials. For the cooled structures in a six-module engine, the mass per unit capture area is 1328 kg/m^2 (259 lb/ft^2). The total mass of a six-module engine assembly including the fuel system is 1577 kg (3477 lb).

This report summarizes the results of the study.

17. Key Words (Suggested by Author(s))
Regeneratively cooled structure
Scramjet
Thermal protection systems
Hypersonic engine

18. Distribution Statement
Unclassified-unlimited

Subject Category 07

19. Security Classif. (of this report)	20. Security Classif. (of this page)	21. No. of Pages	22. Price*
Unclassified	Unclassified	36	$4.50

*For sale by the National Technical Information Service, Springfield, Virginia 22161

NASA-Langley, 1979

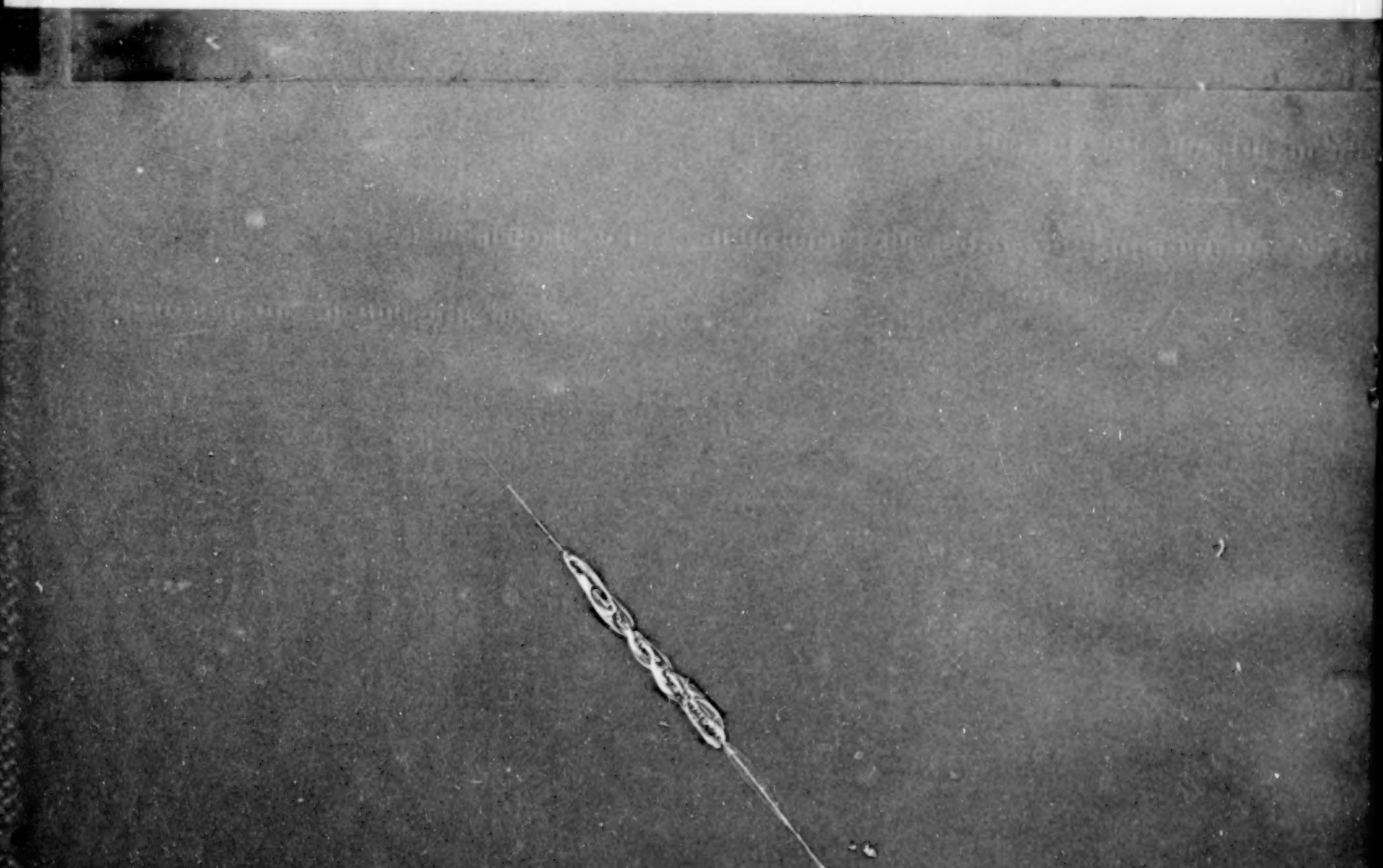

END

May 29, 1981